J. Fluid Mech. (1992), *vol.* 235, *pp.* 349–378
Printed in Great Britain

Homogeneous buoyancy-generated turbulence

By G. K. BATCHELOR[1], V. M. CANUTO[2] AND J. R. CHASNOV[2]

[1] Department of Applied Mathematics and Theoretical Physics, University of Cambridge, Silver Street, Cambridge CB3 9EW, UK

[2] NASA Goddard Institute for Space Studies, 2880 Broadway, New York, NY 10025, USA

(Received 25 April 1991)

We consider the statistically homogeneous motion that is generated by buoyancy forces after the creation of homogeneous random fluctuations in the density of infinite fluid at an initial instant. The mean density is uniform, and density fluctuations are smoothed by molecular diffusion. This turbulent flow system has interesting properties, and shows how self-generated motion contributes to the rate of mixing of an 'active' scalar contaminant.

If nonlinear terms in the governing equations are negligible, there is an exact solution which shows that the history of the motion depends crucially on the form of the buoyancy spectrum near zero wavenumber magnitude (κ). According to this solution the Reynolds number of the motion increases indefinitely, so the linear equations do not remain valid. There are indications of similar behaviour when the nonlinear terms are retained. The value of the three-dimensional buoyancy spectrum function at $\kappa = 0$ is shown to be independent of time, and this points to the existence of a similarity state of turbulence with decreasing mean-square velocity but increasing Reynolds number at large times.

We have made a numerical simulation of the flow field and have obtained the mean-square velocity and density fluctuations and the associated spectra as functions of time for various initial conditions. An estimate of the time required for the mean-square density fluctuation to fall to a specified small value is found. The expected similarity state at large times is confirmed by the numerical simulation, and there are indications of a second similarity state which develops asymptotically when the buoyancy spectrum is zero at $\kappa = 0$. The analytical and numerical results together give a comprehensive description of the birth, life and lingering death of buoyancy-generated turbulence.

1. Introduction

If a random and statistically homogeneous distribution of density of fluid of infinite extent is created by some means, a random and statistically homogeneous motion of the fluid is subsequently generated by buoyancy forces. This motion is resisted by viscous stresses, and the density variation is smoothed by molecular diffusion of the scalar property of the fluid that is associated with the density (e.g. temperature, concentration of solute); and there are nonlinear effects which generate both larger- and smaller-scale components of the scalar quantity and so affect the rate of smoothing. If the Reynolds number of the motion is large, the motion will be turbulent in the ordinary sense of inertia forces being dominant.

This is an intrinsically interesting type of flow, which may be said to be generated by an 'active' conserved scalar quantity. For definiteness we suppose that initially

the fluid is everywhere at rest, with the given distribution of density. The motion then develops by the action of gravity, and since the mean-square density fluctuation can only decrease one would expect an ultimate return to a state of rest of uniform fluid. Buoyancy-generated random motion of this kind has a well-defined birth, lives for a time in which there is a burst of activity, and then presumably dies, partly in consequence of that activity. The source of energy of the motion is the potential energy in the initial state of rest, and the two molecular transport coefficients represent sinks. The expected return to rest may be slow however. For suppose that the advective mixing generates large-scale density variations on which buoyancy forces act to produce large-scale slow-interacting, slowly decaying components of the motion. What is the outcome of this process? Note that the source of potential energy is unlimited when the extent of the fluid in the vertical direction is unlimited.

In this paper we try to elucidate the nature of random buoyancy-driven flow and to provide some numerical data which may be useful in various physical contexts. Our homogeneous buoyancy-driven flow field has been conceived as an idealized system, which, like its simpler relative, namely homogeneous turbulence in uniform fluid, may be useful as a vehicle for the general study of turbulence. We do not know of any attempt to generate a homogeneous buoyancy-driven flow field in the laboratory, or of any relevant observational data. In connection with possible applications, it should be noted that we are concerned here with situations in which the gradient of mean density is zero. The phenomenon of 'fossil turbulence' in the ocean (Gibson 1986), which involves residual velocity and density fluctuations in the presence of a negative vertical gradient of mean density, is thus different although no doubt there are connections. In considerations of the rate of mixing, which here is affected by both molecular diffusion and buoyancy forces, the quantity of interest is likely to be the mean-square density fluctuation as a function of time.

The parameters determining the motion generated from rest by buoyancy forces are easily enumerated. They are, firstly, the statistical parameters needed for the specification of the initial random spatial distribution of fluid density, assumed to be statistically homogeneous; secondly, the two molecular transport coefficients, the kinematic viscosity of the fluid and the diffusivity of the conserved scalar quantity responsible for the spatial variation of fluid density; and thirdly gravity. In order to have an initial state specified by a manageably small number of parameters, we shall later assume simple representative forms for the statistical properties of the initial spatial distribution of density.

The principal specific objectives of our enquiry will be values of the mean-square density fluctuation and the mean-square velocity as functions of time measured from the instant at which the fluid is stationary, for different representative values of the governing dimensionless parameters. The case of large Reynolds number at which the flow is turbulent is of course of greatest interest, and many of our results are concerned with that case. The means of enquiry will be partly theoretical analysis and partly numerical simulation of the flow field.

2. The governing equations

The mass-conservation equation and the equation of motion for fluid of viscosity μ, assumed uniform, are as follows:

$$\frac{\partial \rho}{\partial t} + \boldsymbol{u}\cdot\boldsymbol{\nabla}\rho + \rho\boldsymbol{\nabla}\cdot\boldsymbol{u} = 0, \tag{2.1}$$

$$\rho\left(\frac{\partial \boldsymbol{u}}{\partial t}+\boldsymbol{u}\cdot\boldsymbol{\nabla}\boldsymbol{u}\right)=\rho\boldsymbol{g}-\boldsymbol{\nabla}p+\mu\nabla^2\boldsymbol{u}, \tag{2.2}$$

where ρ, p and $\boldsymbol{u}$ are the fluid density, pressure and velocity. We suppose that density variations are small, relative to the absolute density, and are due to the dependence of ρ on a conserved scalar intensive property of the fluid to be denoted by ϕ (e.g. concentration). Thus we may write

$$\rho=\rho_0+\rho', \quad \phi=\phi_0+\phi',$$

where ρ_0, ϕ_0 are uniform and constant mean values and ρ', ϕ' are fluctuations about the mean related by

$$\rho'=\beta\phi', \tag{2.3}$$

in which β is a constant dependent on the physical meaning of ϕ. With use of the familiar Boussinesq approximation that small density variations affect the flow only through the buoyancy force, (2.1) and (2.2) now become

$$\boldsymbol{\nabla}\cdot\boldsymbol{u}=0, \tag{2.4}$$

$$\frac{\partial \boldsymbol{u}}{\partial t}+\boldsymbol{u}\cdot\boldsymbol{\nabla}\boldsymbol{u}=\frac{\rho'\boldsymbol{g}}{\rho_0}-\frac{\boldsymbol{\nabla}(p-\rho_0\boldsymbol{g}\cdot\boldsymbol{x})}{\rho_0}+\nu\nabla^2\boldsymbol{u}, \tag{2.5}$$

where $\nu=\mu/\rho_0$.

The equation expressing conservation of the scalar quantity that affects the density may be written in terms of ρ' as

$$\frac{\partial \rho'}{\partial t}+\boldsymbol{u}\cdot\boldsymbol{\nabla}\rho'=D\nabla^2\rho', \tag{2.6}$$

where D is the diffusivity of the quantity of which ϕ is the concentration.

Equations (2.4)–(2.6) govern the life and death of our buoyancy-driven flow. At the initial instant, $t=0$, the fluid is at rest and ρ' is a stationary random function of position $\boldsymbol{x}$ with zero mean and other specified statistical properties. At subsequent instants, $\boldsymbol{u}, \rho'$, and $p-\rho_0\boldsymbol{g}\cdot\boldsymbol{x}$ must be stationary random functions of $\boldsymbol{x}$, since there is no agency capable of disturbing the statistical homogeneity.

Our later numerical simulation of the flow field demands non-dimensional variables, and we shall make the transformation now. The explicit lengthscales in the flow system are those characterizing the initial distribution of ρ' statistically. There may be many such lengths, and we select one of them, l_0 say, for the purpose of forming dimensionless variables. (l_0 might be, for example, the wavelength at which the initial spatial spectrum of ρ' has its maximum.) A timescale may be constructed from l_0 and g, but since the gravitational acceleration appears in equation (2.5) effectively only in combination with ρ'/ρ_0, the relevant timescale should be formed from l_0 and the product of g and some statistical measure of the magnitude of ρ'/ρ_0 at $t=0$ which we denote as θ_0 without specifying the precise meaning of θ_0 at this stage.

We now define dimensionless variables (distinguished by capital letters) as follows:

$$T=t\left(\frac{g\theta_0}{l_0}\right)^{\frac{1}{2}}, \quad \boldsymbol{X}=\frac{\boldsymbol{x}}{l_0}, \quad \boldsymbol{U}=\frac{\boldsymbol{u}}{(l_0 g\theta_0)^{\frac{1}{2}}}, \quad P=\frac{p-\rho_0\boldsymbol{g}\cdot\boldsymbol{x}}{\rho_0 l_0 g\theta_0}, \quad \Theta=\frac{\rho' g}{\rho_0 g\theta_0}, \tag{2.7}$$

and Θ will be referred to as the dimensionless buoyancy. Equations (2.4)–(2.6) may then be written in dimensionless form as

$$\boldsymbol{\nabla}\cdot\boldsymbol{U}=0, \tag{2.8}$$

$$\frac{\partial \boldsymbol{U}}{\partial T} + \boldsymbol{U}\cdot\nabla\boldsymbol{U} = j\Theta - \nabla P + \frac{1}{R_0}\nabla^2 \boldsymbol{U}, \tag{2.9}$$

$$\frac{\partial \Theta}{\partial T} + \boldsymbol{U}\cdot\nabla\Theta = \frac{1}{\sigma R_0}\nabla^2 \Theta, \tag{2.10}$$

where $\boldsymbol{j}$ is the vertical (downwards) unit vector, and

$$R_0 = \frac{(l_0^3 g\theta_0)^{\frac{1}{2}}}{\nu}, \quad \sigma = \frac{\nu}{D}. \tag{2.11}$$

Further dimensionless groups may be needed in the specification of the initial conditions.

R_0 as defined above is a pseudo-Reynolds number formed from characteristic length and velocity scales at the initial instant, the velocity scale being that which makes the Froude number (in which g is modified by the magnitude of the density variations) equal to unity; alternatively R_0 can be regarded as proportional to an initial Rayleigh (or Grashof) number to the power half. On the other hand, the Reynolds number of the flow field at time t, R_t say, based on characteristic length and velocity scales of the fluid motion at time t, is a function of t which is zero at $t = 0$ since the fluid is initially at rest. The value of this Reynolds number and the corresponding Péclet number σR_t are important quantities because they indicate the current relative magnitude of the nonlinear terms and the viscous-diffusion terms in (2.9) and (2.10).

3. Solutions of the linearized equations

The scope for analytical deductions from the governing equations is limited, but there are useful exact solutions of the linearized equations which approximate to solutions of the full equations under certain conditions.

3.1. Θ *initially varies in one spatial direction only*

In this case Θ and $\boldsymbol{U}$ continue to vary only in this direction, to which $\boldsymbol{U}$ is orthogonal, and so the nonlinear terms in (2.9) and (2.10) are identically zero. Thus, if Θ initially varies sinusoidally with non-dimensional wavenumber $\boldsymbol{\kappa}$ ($= \boldsymbol{k}l_0$, where $kl_0 = 2\pi$) and amplitude A, the solution to (2.8)–(2.10) is

$$\Theta = A \exp\left(-\frac{\kappa^2 T}{\sigma R_0}\right) \sin \boldsymbol{\kappa}\cdot\boldsymbol{X}, \tag{3.1}$$

$$P = -A\frac{\boldsymbol{\kappa}\cdot\boldsymbol{j}}{\kappa^2} \exp\left(-\frac{\kappa^2 T}{\sigma R_0}\right) \cos \boldsymbol{\kappa}\cdot\boldsymbol{X}, \tag{3.2}$$

$$\boldsymbol{U} = A\frac{\boldsymbol{\kappa}\times(\boldsymbol{j}\times\boldsymbol{\kappa})}{\kappa^4}\frac{\sigma R_0}{1-\sigma}\left\{\exp\left(-\frac{\kappa^2 T}{R_0}\right) - \exp\left(-\frac{\kappa^2 T}{\sigma R_0}\right)\right\} \sin \boldsymbol{\kappa}\cdot\boldsymbol{X}. \tag{3.3}$$

This solution shows that when $T > 0$ plane layers of heavy fluid normal to $\boldsymbol{\kappa}$ slide downwards parallel to themselves without distortion and layers of light fluid slide upwards; meanwhile the spatial variation of Θ is being smoothed out by diffusion, at a rate which is unaffected by the fluid motion. If the diffusivity is zero, a steady unidirectional motion in which gravity and viscous resistance are in balance is established asymptotically. If on the other hand the fluid viscosity is zero, the

motion generated by gravity is unresisted and another, different, steady state survives after the concentration variations have been eliminated by diffusion. If neither ν nor D is zero, $\boldsymbol{U} \to 0$ as $T \to \infty$. The maximum magnitude of $\boldsymbol{U}$ occurs at

$$T = \frac{R_0 \sigma \ln \sigma}{\kappa^2 \sigma - 1}, \quad \boldsymbol{\kappa} \cdot \boldsymbol{X} = \tfrac{1}{2}\pi,$$

and is given by

$$|\boldsymbol{U}|_{\mathrm{m}} = A \frac{|\boldsymbol{\kappa} \times (\boldsymbol{j} \times \boldsymbol{\kappa})|}{\kappa^4} R_0 \sigma^{1/(1-\sigma)}. \tag{3.4}$$

The maximum value of the current Reynolds number R_t for this case of a single Fourier component is evidently of order R_0^2. The mean-square fluctuations $\langle \Theta^2 \rangle$ and $\langle U_3^2 \rangle / R_0^2$, where U_3 is the vertical component of $\boldsymbol{U}$ and the angle brackets denote a volume average, derived from (3.1) and (3.3) are plotted in figure 1 as functions of T/R_0 for various values of σ, for the case in which $\boldsymbol{\kappa}$ is a horizontal vector with magnitude 2π and $A = \sqrt{2}$ (corresponding to the choice $\theta_0 = \langle \rho'^2 / \rho_0^2 \rangle_{t=0}^{\frac{1}{2}}$). The maximum value of the dimensional spatial-mean-square velocity for given $g\theta_0$ is of order k^{-4} and occurs at a dimensional time of order k^{-2}, where k is the dimensional wavenumber magnitude. The vertical buoyancy flux $\langle U_3 \Theta \rangle$ found from (3.1) and (3.3) shows that the coefficient of correlation of U_3 and θ in this unidirectional flow has the notably high value of $(5/6)^{\frac{1}{2}}$, $= 0.91$, for all values of T.

As an illustration of magnitudes, take the case in which the root-mean-square of density fluctuations in water is 1% of the mean density (so that $\theta_0 = 0.01$) and $l_0 = 2\pi/k = 1$ cm, giving $R_0 = 313$; then, if σ has the representative value 10^2–10^3 (in which case the factor containing σ in (3.4) is close to unity) and the wavenumber vector $\boldsymbol{\kappa}$ is horizontal, $|\boldsymbol{U}|_{\mathrm{m}} = 11.1$. This corresponds to a maximum dimensional velocity of 34.8 cm/s. The corresponding Reynolds number of the flow of water with lengthscale 1 cm and velocity 34.8 cm/s is $R_t = 3480$. It is perhaps surprising that seemingly small density fluctuations can generate a flow with moderately large Reynolds number; and much larger values are possible with larger values of l_0 because the maximum of R_t for given $g\theta_0$ is proportional to l_0^3.

The solution can of course be generalized to an arbitrary initial dependence of Θ on $\boldsymbol{\kappa} \cdot \boldsymbol{X}$ by the addition of other Fourier components with wavenumbers parallel to $\boldsymbol{\kappa}$. But when there are two or more Fourier components with non-parallel wavenumbers in the initial Fourier representation of Θ, the nonlinear terms in (2.9) and (2.10) are no longer zero (except at $T = 0$), the different Fourier components interact, and superposition is no longer valid in general.

3.2. *Small values of R_t and σR_t*

In the case of an evolving flow field containing eddies of different lengthscales it is difficult to forecast the values of T at which the nonlinear terms in the governing equations are negligible. However, the nonlinear terms no doubt become negligible as $R_t \to 0, \sigma R_t \to 0$ for given T, and that is what we shall assume here, without concerning ourselves with the appropriate definition of R_t or with prediction of the circumstances in which R_t and σR_t are small. The purpose of this subsection is simply to examine the consequences of the nonlinear terms in (2.9) and (2.10) being small. At the very least the nonlinear terms will be negligible for sufficiently small values of T, because the fluid is stationary at $T = 0$.

When the nonlinear terms in (2.9) and (2.10) are negligible, the different Fourier components of Θ and $\boldsymbol{U}$ behave independently and may be superimposed. The

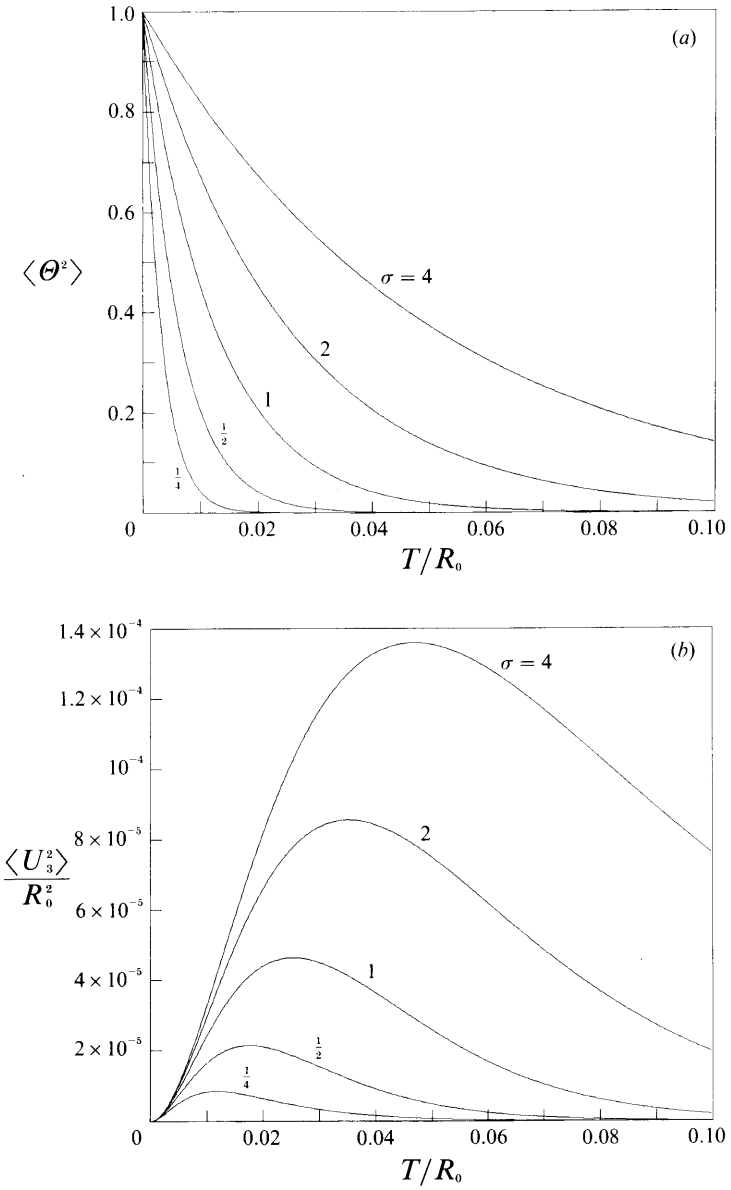

FIGURE 1. Analytical results for a sinusoidal distribution of Θ and various values of σ: (*a*) $\langle \Theta^2 \rangle$ *vs.* T/R_0, (*b*) $\langle U_3^2 \rangle / R_0^2$ *vs.* T/R_0.

behaviour of the Fourier component with wavenumber $\boldsymbol{\kappa}$ is given by (3.1) and (3.3), and we may construct from these relations the corresponding expressions for the spectra of Θ and $\boldsymbol{U}$. We define $\Psi(\boldsymbol{\kappa}, t)$ and $\Phi_{ij}(\boldsymbol{\kappa}, t)$ as spectral densities in wavenumber space, that is, as three-dimensional Fourier transforms of the covariances $\langle \Theta(\boldsymbol{X})\Theta(\boldsymbol{X}+\boldsymbol{r}) \rangle$ and $\langle U_i(\boldsymbol{X})U_j(\boldsymbol{X}+\boldsymbol{r}) \rangle$, where the angle brackets denote a volume average. It then follows from (3.1) that

$$\Psi(\boldsymbol{\kappa}, T) = \Psi(\boldsymbol{\kappa}, 0) \exp\left(-\frac{2\kappa^2 T}{\sigma R_0}\right) \tag{3.5}$$

and $$\langle \Theta^2 \rangle = \int \Psi(\boldsymbol{\kappa}, T)\, \mathrm{d}\boldsymbol{\kappa} = \int_0^\infty G(\kappa, T)\, \mathrm{d}\kappa = \int_0^\infty G(\kappa, 0) \exp\left(-\frac{2\kappa^2 T}{\sigma R_0}\right) \mathrm{d}\kappa, \tag{3.6}$$

where $G(\kappa, T)$ is the integral of the buoyancy spectrum function over a spherical surface of radius κ in wavenumber space. For simplicity we take the initial distribution of Θ to be statistically isotropic, in which case it remains isotropic for all T (in the linear range) and

$$G(\kappa, T) = 4\pi\kappa^2 \Psi(\boldsymbol{\kappa}, T). \tag{3.7}$$

The velocity distribution is then statistically symmetrical about the vertical (X_3) axis, and (3.3) shows that

$$8\langle U_1^2 \rangle = 8\langle U_2^2 \rangle = \langle U_3^2 \rangle = \frac{8\sigma^2 R_0^2}{15(1-\sigma)^2} \int_0^\infty G(\kappa, 0) \left\{ \exp\left(-\frac{\kappa^2 T}{R_0}\right) - \exp\left(-\frac{\kappa^2 T}{\sigma R_0}\right) \right\}^2 \frac{\mathrm{d}\kappa}{\kappa^4}. \tag{3.8}$$

There is a paradox associated with the expression (3.8) for the mean-square velocity caused by gravity acting on a density distribution which has a continuous spectrum of superimposed non-interacting Fourier components. The relations (3.3) and (3.4) for a single Fourier component with wavenumber $\boldsymbol{\kappa}$ show that the fluid velocity magnitude is zero initially and increases with T to a maximum which is proportional to κ^{-2} after a time of order κ^{-2} before decreasing to zero. Thus, if the initial spectrum of the buoyancy distribution contains components with small wavenumber, the velocity of the fluid is correspondingly large. An attempt to calculate the velocity due to buoyancy forces acting on fluid whose density is a stationary random function of position with a continuous spectrum extending to zero wavenumber may encounter a divergence if the calculation is based on the linearized equations, as (3.8) is.

We see this explicitly by evaluating the integral in (3.8) asymptotically as $T \to \infty$. The three-dimensional spectral density $\Psi(\boldsymbol{\kappa}, T)$ is in general an even function of $\boldsymbol{\kappa}$, and so we may write

$$G(\kappa, 0) = 4\pi\kappa^2 (C_0 + C_2 \kappa^2 + \ldots) \tag{3.9}$$

near $\kappa = 0$, where $C_0, C_2, \ldots$ are constants determined by the initial generation of the density fluctuations, C_0 being the value of the three-dimensional spectral density $\Psi(\boldsymbol{\kappa}, 0)$ at $\kappa = 0$. Note from (3.5) and (3.7) that such an expansion for G at any non-zero value of T would likewise begin with the term $4\pi C_0 \kappa^2$, or if $C_0 = 0$ with the term $4\pi C_2 \kappa^4$. As $T \to \infty$ the integral becomes dominated by small values of κ, and

$$\langle U_3^2 \rangle \approx \frac{32\pi\sigma^2 R_0^2}{15(1-\sigma)^2} \left\{ C_0 \left(\frac{T}{R_0}\right)^{\frac{1}{2}} I_0 + C_2 \left(\frac{R_0}{T}\right)^{\frac{1}{2}} I_2 + \ldots \right\}, \tag{3.10}$$

where $$I_0 = \int_0^\infty \eta^{-2} (\mathrm{e}^{-\eta^2} - \mathrm{e}^{-\eta^2/\sigma})^2 \, \mathrm{d}\eta, \quad I_2 = \int_0^\infty (\mathrm{e}^{-\eta^2} - \mathrm{e}^{-\eta^2/\sigma})^2 \, \mathrm{d}\eta.$$

Thus as $T \to \infty$ the mean-square velocity fluctuation diverges as $T^{\frac{1}{2}}$ when $C_0 \neq 0$, because more and more of the small-wavenumber Fourier components develop a maximum velocity which increases as κ^{-2}. If however $C_0 = 0$, but $C_2 \neq 0$, the asymptotic behaviour of $\langle U_3^2 \rangle$ is as $T^{-\frac{1}{2}}$.

Use of the linearized equations thus leads to a divergent mean-square velocity fluctuation as $T \to \infty$ when $C_0 \neq 0$, which is incompatible with neglect of the

nonlinear terms in the governing equations. And even when $C_0 = 0$ but $C_2 \neq 0$ it may be shown that there is the same inconsistency, because the lengthscale of the components making the major contribution to the kinetic energy and the density variance then increases as $T^{\frac{1}{2}}$ and so leads to an indefinitely increasing current Reynolds number of the flow. We thus reach the surprising conclusion that, however small the initial density fluctuation may be, the linearized equations do not remain valid indefinitely if at least one of C_0 and C_2 is non-zero. Ultimately the nonlinear terms become significant. However, if both C_0 and C_2 are zero, the Reynolds number decreases and the linearized equations do remain self-consistent.

The conclusion that $\langle U_3^2 \rangle \to \infty$ as $T \to \infty$ when $C_0 \neq 0$ would of course be affected by the presence of walls bounding the fluid. If these walls have linear dimensions d, no density components with lengthscales larger than d can be created at the initial instant. There is then a finite limit to the maximum velocity that can be generated in the fluid, according to the linearized equations, which may be seen from (3.4) to be proportional to d^2. However, a more interesting possibility is that the divergence in the value of $\langle U_3^2 \rangle$ is cut off by the effects of the nonlinear terms in (2.9) and (2.10), which become significant when R_t and σR_t are no longer small. Later we shall describe a numerical simulation of the flow field intended to throw light on these nonlinear effects.

4. The large-scale components of Θ and U

It has been seen that the asymptotic ($T \to \infty$) behaviour of the flow field is determined, according to the linearized equations, by the form of the spectrum of Θ at small wavenumber magnitude at $T = 0$, the reason being that those small-wavenumber components of density fluctuation decay more slowly and generate larger fluid velocities. It is not obvious that this remains true when the nonlinear terms are retained in the governing equations, because the different Fourier components do not then develop buoyancy-driven motions independently and the effect of nonlinear transfer may be to hasten or hinder decay of the small-wavenumber components. However, it seems likely that these large-scale components play an important role in the asymptotic dynamics, especially if, as in the case of homogeneous turbulence in a uniform fluid, there are some invariant properties of the big eddies which relate the asymptotic behaviour of the flow field to its statistical properties at the initial instant. We therefore consider here the consequences of the full governing equations (2.8)–(2.10) for the Fourier components of Θ and $\boldsymbol{U}$ at small wavenumber magnitudes.

There are some existing results for the velocity spectrum of decaying homogeneous turbulence in fluid of uniform density which give us some guidance, two of the relevant references being Batchelor & Proudman (1956) and Saffman (1967). Saffman pointed out that any homogeneous turbulent flow may be regarded as having been generated by an impulsive body force $\boldsymbol{f}(\boldsymbol{X})$ per unit mass applied to the fluid at some (virtual) initial instant. He showed that, if all integral moments of cumulants of the random force $\boldsymbol{f}$ exist, then so too do those of the fluid vorticity at the initial instant, and the velocity spectral tensor $\Phi_{ij}(\boldsymbol{\kappa})$ (the Fourier transform of the velocity covariance $\langle U_i(\boldsymbol{X})\, U_j(\boldsymbol{X}+\boldsymbol{r}) \rangle$) is of the following form at small values of the wavenumber magnitude κ at all later times:

$$\Phi_{ij}(\boldsymbol{\kappa}, T) = \left(\delta_{i\alpha} - \frac{\kappa_i \kappa_\alpha}{\kappa^2}\right)\left(\delta_{j\beta} - \frac{\kappa_j \kappa_\beta}{\kappa^2}\right) M_{\alpha\beta} + o(1), \tag{4.1}$$

where δ_{ij} is the unit second-rank tensor and the coefficient $M_{\alpha\beta}$ is independent of T. Earlier, Batchelor & Proudman (1956) had supposed that the kind of homogeneous turbulence that is generated by placing a grid of bars across a uniform stream of fluid would be such that all integral moments of cumulants of the velocity converge at the initial instant; and they showed that for this kind of homogeneous turbulence the form of $\Phi_{ij}(\boldsymbol{\kappa})$ at small κ is

$$\Phi_{ij}(\boldsymbol{\kappa}, T) = \left(\delta_{i\alpha} - \frac{\kappa_i \kappa_\alpha}{\kappa^2}\right)\left(\delta_{j\beta} - \frac{\kappa_j \kappa_\beta}{\kappa^2}\right)\kappa_k \kappa_l M_{\alpha\beta kl} + O(\kappa^3 \ln \kappa), \tag{4.2}$$

in which the coefficient $M_{\alpha\beta kl}$ is not independent of T in general. The relation between these two results was made clear by Saffman, who showed that the restriction on the velocity cumulants at the initial instant imposed by Batchelor & Proudman is equivalent to requiring both that the impulsive body force $\boldsymbol{f}$ have convergent integral moments of cumulants and that it be a solenoidal function of position.

Inasmuch as a gravitational body force acting on fluid of non-uniform density is not solenoidal in general, it seems likely that the asymptotic form of the velocity spectral tensor in our buoyancy-driven turbulence will resemble (4.1); although since the non-solenoidal body force here acts continuously, and not as an impulse at the initial instant alone, we cannot expect the coefficient $M_{\alpha\beta}$ to be constant.

Analogous results for the spectral density of the buoyancy force at small κ may be obtained directly from the (full) governing equations. The expression for the rate of change of the mean of the product of $\Theta(\boldsymbol{X})$ and $\Theta(\boldsymbol{X}')$ obtained from (2.10) is

$$\frac{\partial \langle \Theta \Theta' \rangle}{\partial T} = \nabla_{\boldsymbol{r}} \cdot \langle \boldsymbol{U}\Theta'\Theta - \boldsymbol{U}'\Theta'\Theta \rangle + \frac{2}{\sigma R_0} \nabla_{\boldsymbol{r}}^2 \langle \Theta \Theta' \rangle, \tag{4.3}$$

where Θ', $\boldsymbol{U}'$ stand for $\Theta(\boldsymbol{X}')$, $\boldsymbol{U}(\boldsymbol{X}')$ and $\boldsymbol{r} = \boldsymbol{X}' - \boldsymbol{X}$. The three-dimensional Fourier transform of this relation is

$$\frac{\partial \Psi(\boldsymbol{\kappa}, T)}{\partial T} = \boldsymbol{\kappa} \cdot \boldsymbol{V}(\boldsymbol{\kappa}, T) - \frac{2\kappa^2}{\sigma R_0} \Psi(\boldsymbol{\kappa}, T), \tag{4.4}$$

where $\boldsymbol{V}(\boldsymbol{\kappa}, T)$ is the Fourier transform of a third-order two-point product of $\boldsymbol{U}$ and Θ which can be expected to be regular at $\boldsymbol{\kappa} = 0$. This equation shows that the first time derivative of $\Psi(\boldsymbol{\kappa}, T)$ vanishes at $\boldsymbol{\kappa} = 0$, and it seems, from the form of the terms in the two rate-of-change equations (2.9) and (2.10), that the same is true of repeated time derivatives.

We thus have the important result that the parameter C_0 appearing in the relation

$$\lim_{\kappa \to 0} \Psi(\kappa, T) = C_0, \quad \text{or} \quad G(\kappa, T) \sim 4\pi C_0 \kappa^2 \quad \text{for small } \kappa, \tag{4.5}$$

is an invariant which takes for all T the value that is prescribed at the initial instant. This was obviously so in the period of validity of the linearized equations, and now we see it to be true generally. An additional result which follows from the equation of motion (2.9) is that there is a direct contribution to $\partial \Phi_{ij}/\partial T$, representing the generation of motion on a scale $2\pi/\kappa$ due to buoyancy, which in general is not small near $\kappa = 0$, showing that the asymptotic form of Φ_{ij} is of order κ^0 for small κ and is not constant, in line with our expectation above.

The invariance of C_0 can be understood physically by adapting an argument used by Saffman (1967) to show the invariance of the leading term in his expression for

the energy-spectrum tensor at small wavenumber magnitude in the case of homogeneous turbulence in fluid of uniform density. By definition of $\Psi(\boldsymbol{\kappa}, T)$ we have

$$\Psi(0,T) = \frac{1}{8\pi^3}\int \langle \Theta(\boldsymbol{X},T)\,\Theta(\boldsymbol{X}+\boldsymbol{r},T)\rangle \,\mathrm{d}\boldsymbol{r},$$

$$= \frac{1}{8\pi^3}\lim_{V\to\infty}\left\{\frac{1}{V^{\frac{1}{2}}}\int_V \Theta(\boldsymbol{X},T)\,\mathrm{d}\boldsymbol{X}\right\}\left\{\frac{1}{V^{\frac{1}{2}}}\int_V \Theta(\boldsymbol{X}+\boldsymbol{r},T)\,\mathrm{d}\boldsymbol{r}\right\} \tag{4.6}$$

in view of the equivalence of ensemble mean values and spatial averages. Now each of these two integrals in the last line of (4.6) changes with time as a consequence of diffusion and convection of fluid mass across the surface bounding V, and since these are random processes with characteristic lengthscales small compared with $V^{\frac{1}{3}}$ the rate of change of each integral is proportional to the square root of the area of this surface, that is, to $V^{\frac{1}{3}}$; and so $\Psi(0,T)$, $= C_0$, is constant. This argument is applicable to the small-wavenumber limit of the spectrum of the amount per unit volume of any conserved quantity. The conserved quantity in Saffman's paper was fluid momentum, and here it is fluid mass.

The possibility that the initial conditions are such that $C_0 = 0$ should also be considered. Now the integral of $\langle \boldsymbol{U}\Theta'\Theta - \boldsymbol{U}'\Theta'\Theta\rangle$ with respect to $\boldsymbol{r}$ over all space is clearly zero, showing that the Fourier transform $V(\boldsymbol{\kappa}, T)$ (see (4.4.)) is zero at $\boldsymbol{\kappa} = 0$. It appears therefore that a contribution to $\Psi(\boldsymbol{\kappa}, T)$ of order κ^2 (and to $G(\kappa, T)$ of order κ^4) is generated by nonlinear dynamical processes. We have also reached this conclusion by expanding the Fourier coefficients of Θ and $\boldsymbol{U}$ in powers of T and supposing that the Fourier coefficients of Θ are normally distributed at $\boldsymbol{T} = 0$ (which in fact coincides with the assumption made in our later numerical simulation); and this calculation provides the additional information that the contribution generated dynamically is essentially positive. Hence when $C_0 = 0$ the form of $G(\kappa, T)$ near $\kappa = 0$ is, in general,

$$G(\kappa, T) \sim 4\pi C_2 \kappa^4, \tag{4.7}$$

where C_2 depends on T. Note that there is no reason to expect the contribution to $\Psi(\boldsymbol{\kappa}, T)$ of order κ^2 that is generated dynamically to be isotropic, even when $\Psi(\boldsymbol{\kappa}, 0)$ is.

The order of magnitude of $\Phi_{ij}(\boldsymbol{\kappa}, T)$ at small κ is also different when $C_0 = 0$. The direct contribution to $\partial\Phi_{ij}/\partial T$ due to the generation of motion by buoyancy forces is the Fourier transform of

$$j_i\langle\Theta U_j'\rangle + j_j\langle\Theta' U_i\rangle, \tag{4.8}$$

and the value of each of these two Fourier transforms at $\kappa = 0$ may be written as the product of two integrals in the manner of (4.6). But (4.6) shows that when $C_0 = 0$

$$\lim_{V\to\infty}\left\{\frac{1}{V^{\frac{1}{2}}}\int_V \Theta(\boldsymbol{X},T)\,\mathrm{d}\boldsymbol{X}\right\} = 0, \tag{4.9}$$

and hence the contribution to $\partial\Phi_{ij}/\partial T$ due to the generation of motion by buoyancy forces is also zero at $\kappa = 0$. The spherically integrated energy spectrum

$$E(\kappa, T) = \frac{1}{2}\int \Phi_{ij}(\boldsymbol{\kappa})\,\mathrm{d}A(\boldsymbol{\kappa}) \tag{4.10}$$

can be expanded as a power series in κ^2, and when $C_0 = 0$ its form near $\kappa = 0$ is thus

$$E(\kappa, T) \propto \kappa^4, \tag{4.11}$$

in which the constant of proportionality depends on T.

$G(\kappa, 0)$	$G(\kappa, T)$	$E(\kappa, T)$
$4\pi C_0 \kappa^2$	$4\pi C_0 \kappa^2$	$\sim \kappa^2$
$4\pi C_2 \kappa^4$	$\sim \kappa^4$	$\sim \kappa^4$
$4\pi C_{2n} \kappa^{2(n+1)}$ $(n > 1)$	$\sim \kappa^4$	$\sim \kappa^4$

TABLE 1. Asymptotic forms of the functions $G(\kappa, T)$ and $E(\kappa, T)$ as $\kappa \to 0$ for a given initial form of $G(\kappa, T)$. Only the coefficient C_0 is constant.

Table 1 shows the various results obtained above for the asymptotic forms, as $\kappa \to 0$, of the directionally integrated spectra of buoyancy and velocity.

An asymptotic similarity state

The results of §§3 and 4 taken together point strongly to the existence of an interesting and unexpected similarity state of the flow field as $T \to \infty$, for those initial conditions for which the constant C_0 defined in (4.5) is non-zero.

We saw in §3.2 that as T increases from zero the fluid velocity increases from zero and, provided the velocity remains so small that the nonlinear terms in the governing equations are negligible, the flow field becomes dominated by the large-scale Fourier components of $\boldsymbol{\Theta}$, these being the slowest to decay and the most effective in generating motion due to gravity. The product of the root-mean-square velocity and the lengthscale of the energy-containing eddies was found to increase indefinitely provided at least one of the constants C_0 and C_2 in (3.9) is non-zero, according to the linearized equations, so it is inevitable that nonlinear terms ultimately become significant. The effects of viscosity and diffusion are then supplemented and replaced by nonlinear transfer processes which are difficult to treat analytically, but it is a reasonable supposition that, as in the linear regime, the values of $\langle \boldsymbol{\Theta}^2 \rangle$ and $\langle \boldsymbol{U}^2 \rangle$ become dominated by Fourier components with wavenumbers near $\kappa = 0$. The influence of the initial conditions on the flow field is thus ultimately confined to the parameters specifying the form of $\boldsymbol{\Psi}(\boldsymbol{\kappa}, 0)$ near $\kappa = 0$, that is, to the parameter C_0 which is an invariant of the motion. The flow field depends asymptotically ($T \to \infty$) only on T and C_0; and not on R_0 and σ, because, as will be seen, R_l increases indefinitely in the nonlinear regime also.

Dimensional analysis now enables us to determine the similarity laws giving the statistical parameters of the flow field as powers of T in the asymptotic state. It will be recalled that all our variables are non-dimensional, and were made so using two unspecified dimensional parameters l_0 and $g\theta_0$ characteristic of the initial state. In the asymptotic state only one parameter of the initial conditions is relevant, namely the parameter C_0 defined in (4.5), of which the dimensional form is

$$c_0 = g^2 \theta_0^2 l_0^3 C_0. \tag{4.12}$$

We therefore choose $g\theta_0$ to be $(c_0/l_0^3)^{\frac{1}{2}}$, so that $C_0 = 1$ (as it should be when parameters are made dimensionless using c_0 and t), and the power-law dependences of the various statistical parameters on T must now be such that l_0 cancels from their dimensional forms. In this way we find

$$g^2 \langle \rho'^2/\rho_0^2 \rangle \propto c_0^{\frac{2}{5}} t^{-\frac{12}{5}}, \quad \langle \boldsymbol{u}^2 \rangle \propto c_0^{\frac{2}{5}} t^{-\frac{2}{5}}, \quad l_t \propto c_0^{\frac{1}{5}} t^{\frac{4}{5}} \tag{4.13}$$

in the asymptotic state, where l_t is the (dimensional) characteristic lengthscale of the

current distributions of Θ and U. The corresponding relations in terms of non-dimensional variables are

$$\langle \Theta^2 \rangle \propto T^{-\frac{12}{5}}, \quad \langle U^2 \rangle \propto T^{-\frac{2}{5}}, \quad L_t \propto T^{\frac{4}{5}}, \tag{4.14}$$

and each of the spectral densities $G(\kappa, T)$ and $E(\kappa, T)$ is a self-similar function of κ at different times, with lengthscales which vary as $T^{\frac{4}{5}}$, that is

$$G(\kappa, T) = T^{-\frac{8}{5}} \hat{G}(\hat{\kappa}), \quad E(\kappa, T) = T^{\frac{2}{5}} \hat{E}(\hat{\kappa}), \quad \hat{\kappa} = T^{\frac{4}{5}} \kappa. \tag{4.15}$$

The paradox of an ever-increasing mean-square velocity that we encountered in §3.2 for the case in which $G(\kappa, 0)$ is of order κ^2 and the motion is governed by the linearized equations thus no longer occurs when the nonlinear interaction of Fourier components is allowed for, but a vestige of the paradox survives inasmuch as the current Reynolds number increases indefinitely as $T^{\frac{3}{5}}$.

Evidence for the existence of this asymptotic similarity state from a numerical simulation of the flow field will be presented later.

In the case when the initial conditions are such that $C_0 = 0$, $G(\kappa, t)$ behaves as $4\pi C_2 \kappa^4$ for small κ, where C_2 is in general a function of T. It seems that there is here no invariant quantity on which to base an asymptotic similarity state. However, our numerical simulation indicates unexpectedly, that another similarity state with increasing current Reynolds number of the turbulence is established asymptotically, at least approximately.

5. Numerical simulation of the flow field

Our numerical simulations of equations (2.4)–(2.6) have been performed using a pseudo-spectral code for homogeneous turbulence developed by Rogallo (1981). The spatial derivatives of the velocity and density fields are computed in wavenumber space whereas the bilinear products in the convective terms are computed in physical space through use of fast Fourier transforms. The aliasing errors which result are removed by masking and phase-shifting the fields. The fields are time-advanced in wavenumber space and the time-stepping scheme used is second-order Runge–Kutta. Viscous and diffusive terms are treated by use of an integrating factor. A fixed time step Δt, chosen sufficiently small to reproduce accurately the analytical results of the linear analysis, is used to generate initial velocity fluctuations, after which smaller values of Δt, required by the nonlinear terms, are determined by equating to unity the Courant number $U_{\max} \Delta t / \Delta x$, where $U_{\max}$ is the maximum over all grid points of the sum of the absolute values of the three velocity components, and Δx is the distance between grid points.

A representation of the velocity and density fields in Fourier space is achieved by assuming the fields to be periodic with periodicity length 2π. This results in a discrete wavenumber spectrum with each component of the computational wavenumber taking the values $0, \pm 1, \pm 2, \ldots, \pm(\frac{1}{2}N - 1)$, where N is the number of grid points in each of the three directions. The value of N^3 is usually called the resolution of the simulation. Eliminating the aliasing errors in the Rogallo code further restricts the computational wavenumber to a magnitude less than $(\sqrt{2}/3)N$. The simulations presented here are of resolution 64^3 or 128^3. A complete simulation of the birth and death of high-Reynolds-number buoyancy-generated turbulence with resolution 128^3 takes on the order of 15 cpu hours on a single processor of a Cray-YMP, whereas a 64^3 simulation takes on the order of 1 cpu hour.

5.1. *The initial conditions*

The statistical properties of the density field are assumed to be homogeneous and isotropic at the initial instant, and the fluid is stationary, so the initial conditions of our flow field may be completely determined statistically by the initial buoyancy spectrum $G(\kappa,0)$, defined in (3.6). The individual Fourier components of the initial buoyancy field are given by

$$\left\{\frac{G(\kappa,0)}{4\pi\kappa^2}\right\}^{\frac{1}{2}} \exp\,(\mathrm{i}2\pi\omega_{\boldsymbol{\kappa}}) \exp\,(\mathrm{i}\boldsymbol{\kappa}\cdot\boldsymbol{X}),$$

where $\omega_{\boldsymbol{\kappa}}$ is a number between 0 and 1 chosen at random for each wavenumber $\boldsymbol{\kappa}$ under the constraint that change of sign of $\boldsymbol{\kappa}$ gives the complex conjugate, as required by the reality of the density field. To obtain accurate statistics from this particular realization of the density field, a sufficiently large sample of Fourier components must be excited initially.

The initial conditions may result in the introduction of dimensionless groups additional to those specified in (2.11). For simplicity we keep these additional groups to a minimum. In particular, no new dimensionless groups are needed if $G(\kappa,0)$ can be completely specified in terms of the lengthscale l_0 and the statistical measure of the magnitude of the fluctuations in the buoyancy, $g\theta_0$, these being the two dimensional quantities used in the non-dimensionalization (2.7). However, we have seen in §4 that the power-law dependence of $G(\kappa,0)$ on κ at small κ plays a crucial role in the behaviour of the flow at large times. Accordingly, we take as our initial buoyancy spectrum

$$G(\kappa,0) = \frac{A_n}{2\pi}\left\{\frac{\kappa}{2\pi}\right\}^n \exp\,[-\tfrac{1}{2}n(\kappa/2\pi)^2], \tag{5.1}$$

which has been chosen so that $G(\kappa,0)$ has a maximum at $\kappa = 2\pi$. Furthermore, the normalization constant A_n is chosen so that the root-mean-square density fluctuation at $T = 0$ is unity:

$$A_n = \left[\frac{2}{\pi}\right]^{\frac{1}{2}} \frac{n^{\frac{1}{2}(n+1)}}{1\cdot 3\cdot \ldots \cdot (n-1)}. \tag{5.2}$$

Clearly (5.1) introduces a single additional (non-dimensional) parameter to the problem, namely n, the power-law exponent of $G(\kappa,0)$ as $\kappa \to 0$. In the limit of very large n, this additional parameter becomes irrelevant and (5.1) becomes

$$G(\kappa,0) = \delta(\kappa - 2\pi), \tag{5.3}$$

where δ is the Dirac delta-function.

5.2. *Subgrid modelling*

The largest simulations presented here, those with 128^3 resolution, resolve a span of wavenumber magnitudes between unity and 60. Such a range of resolvable scale sizes restricts exact numerical solution of the fundamental equations by a direct numerical simulation to low Reynolds and Péclet numbers, where there are only narrow ranges of dynamically interacting velocity and density scales. However, for flows at high Reynolds or Péclet numbers scales may be excited which are smaller than those represented in the simulation, and the effect of these scales on the computationally resolved scales must be modelled by a subgrid model. The use of a good subgrid model in principle allows accurate statistics to be obtained from a large-eddy simulation for arbitrary Reynolds and Péclet numbers.

Simulations performed here with both R_0 and σR_0 greater than a few hundred require a subgrid model for both the velocity and density fields. A minimum requirement of any subgrid model is to remove the excess energy and density-variance which accumulate at the smallest resolved scales of the simulation. If this excess energy and density-variance is not removed, then the solution of the truncated Fourier series representing the turbulent fields will tend towards an equilibrium equipartition spectrum rather than the desired turbulent solution. However, a good subgrid model should do more than just remove the excess energy and density-variance. It should attempt to model the interactions which actually occur between the subgrid scales and the resolved scales. The introduction of a subgrid model into a simulation is always somewhat *ad hoc*, so that confidence in a statistical result obtained from large-eddy simulation depends on whether the particular result is robust to small changes in the subgrid model.

The large-eddy simulations presented here were performed using a well-known spectral eddy-viscosity and eddy-diffusivity subgrid model (see Kraichnan 1976; Chollet & Lesieur 1981; Chollet 1985; Lesieur & Rogallo 1989) to remove energy and density-variance from the resolved scales. For the eddy viscosity and eddy diffusivity we adopt, respectively,

$$\nu_e(\kappa\,|\,\kappa_m, T) = \{0.145 + 5.01 \exp[-3.03(\kappa_m/\kappa)]\}[E(\kappa_m, T)/\kappa_m]^{\frac{1}{2}} \tag{5.4}$$

and

$$D_e(\kappa\,|\,\kappa_m, T) = \nu_e(\kappa\,|\,\kappa_m, T)/\sigma_e, \tag{5.5}$$

where κ_m is the maximum wavenumber magnitude of the simulation and σ_e is an eddy Schmidt number, assumed here to be constant and equal to 0.6. The eddy viscosity (5.4) differs slightly from that used most recently by Lesieur & Rogallo in that it has been rescaled to coincide with a Kolmogorov inertial-subrange constant equal to 2.1, as computed by Chasnov (1991).

Simulations were performed to determine the sensitivity of our high-Reynolds-number results to the above subgrid model by varying the range of wavenumbers between the peak of the initial density spectrum and the maximum resolved wavenumber of the simulation. We found that the eddy-viscosity and eddy-diffusivity plateau 0.145 in (5.4) tended to overdamp the flow fields at early times, so that for the simulations with $G(\kappa, 0) = \delta(\kappa - 2\pi)$ presented in §6 the eddy-viscosity and eddy-diffusivity plateau 0.145 in (5.4) was set to zero, whereas the cusp contribution 5.01 was unchanged. This modified subgrid model then simply removes the excess energy and density-variance which accumulates at the largest wavenumbers of the simulation without appreciably affecting Fourier components at lower wavenumbers. We believe that use of this modified subgrid model yields the most accurate results for the maximum mean-square velocity fluctuation generated in the fluid. The complete eddy-viscosity and eddy-diffusivity subgrid model is employed for the simulation of the decay of velocity fluctuations in §7. There we are interested in the long-time behaviour of the flow, so that the plateau represents an important physical effect.

Furthermore, we note that use of a modified eddy-viscosity model with stochastic backscatter (Chasnov 1991) did not appreciably affect the statistics of interest to us here. We should note also that although the spectral eddy-viscosity and -diffusivity model given by (5.4) and (5.5) was developed for isotropic turbulence, we have used it to simulate axisymmetric turbulence, and this may result in additional errors. The same form of the eddy-viscosity and -diffusivity model has been used for a large-eddy simulation of a homogeneous axisymmetric stratified flow by Métais & Chollet (1989).

Finally, we note that the simulations performed at values of R_0 and σR_0 of a few hundred or less are essentially fully resolved, and that the statistics obtained from these direct numerical simulations already demonstrate trends which are smoothly continued as we increase R_0 and σR_0 to values where the subgrid model begins to remove substantial energy and scalar variance from the resolved scales.

5.3. *Visualization of the density distribution*

Figure 2 (plate 1) shows visually the numerically calculated dimensionless buoyancy $\Theta(\boldsymbol{X})$ at four different times in the flow evolution for the case $R_0, \sigma R_0 \to \infty$ and $G(\kappa, 0) = \delta(\kappa - 2\pi)$. The gravitational force causes the denser fluid (blue) to fall and the less dense fluid (red) to rise. Only three sides of the periodic computational box are shown on the colour plate. The random density distribution at $T = 0$ subsequently results in a random motion of the fluid ($T = 0.8$), and in the development of more complicated plume-like structures ($T = 1.2$). At even later times ($T = 2.0$), substantial mixing of the initial density fluctuations is observed to occur. Although flow visualization does not yield quantitative statistical results, it may be worthwhile to try to identify some of the features present in the numerical simulation at times within the similarity range, especially those in the velocity field. Unfortunately, present circumstances require us to postpone such a study to a later date.

6. Numerical results for an initial density spectrum characterized by a single length

We present here some quantitative results for the initial density spectrum $G(\kappa, 0) = \delta(\kappa - 2\pi)$. This initial spectrum can be reasonably approximated by (5.1) with $n = 64$. In performing the numerical simulation, the maximum of the initial density spectrum occurs at a computational wavenumber magnitude $k_p = 8$ (so that $l_0 = 2\pi/k_p$ is used to non-dimensionalize the computational results). This choice of k_p was based on two conflicting requirements: that adverse effects of subgrid modelling be limited, implying a value of k_p as small as possible, and that the imposed periodicity length be much larger than any integral scale of the flow, implying a value of k_p as large as possible. The latter requirement also restricts the time integration to relatively short times.

Our simulations are for various values of the pseudo-Reynolds number R_0 and for Schmidt numbers $\sigma = 0.1$, 1.0, and 10.0. The results for $\langle \Theta^2 \rangle$ and $\langle U^2 \rangle$ ($= \langle \boldsymbol{U} . \boldsymbol{U} \rangle$), computed from the grid-scale fluctuations as functions of time for $\sigma = 1.0$ and for R_0 varying from 32 to ∞, are shown in figure 3. The density variance $\langle \Theta^2 \rangle$ versus T approaches a universal curve asymptotically as $R_0 \to \infty$ (figure 3*a*). At large values of R_0, $\langle \Theta^2 \rangle$ is conserved for small times, after which it rapidly cascades to the subgrid scales where it is diminished by molecular diffusion. The time τ required for $\langle \Theta^2 \rangle$ to fall to 0.05 of its initial value at large R_0 is found to be $\tau = 3.1$, and the dimensional form of this useful measure of mixing time is

$$\frac{3.1 l_0^{\frac{1}{2}}}{g^{\frac{1}{2}} \langle \rho'^2 / \rho_0^2 \rangle_{t=0}^{\frac{1}{4}}}, \tag{6.1}$$

where l_0 is the wavelength characteristic of the initial Fourier components. The maximum value attained by the mean-square velocity of the fluid ($\langle U^2 \rangle_{\mathrm{m}}$) is observed to increase monotonically with increasing R_0 and to approach 1.2 asymptotically at a time $T_{\mathrm{m}} = 1.8$ (figure 3*b*). This is in striking contrast to the solutions of the linearized equations in §3, where it was shown that $\langle U^2 \rangle_{\mathrm{m}}$ grows indefinitely like R_0^2

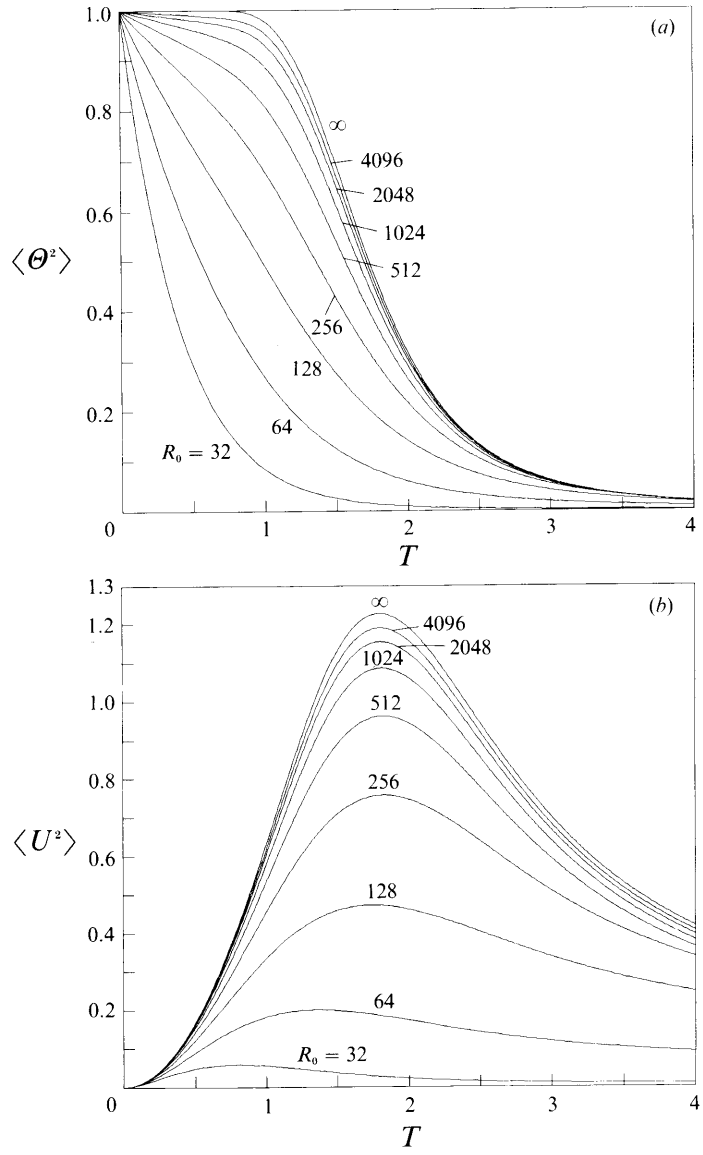

FIGURE 3. Numerical results for the isotropic initial buoyancy spectrum $G(\kappa, 0) = \delta(\kappa - 2\pi)$, for $\sigma = 1.0$ and various values of R_0: (*a*) $\langle \Theta^2 \rangle$ *vs.* T, (*b*) $\langle U^2 \rangle$ *vs.* T.

with increasing R_0. Our asymptotic result provides the following estimate for the dimensional maximum mean-square velocity fluctuation attained in a high-Reynolds-number buoyancy-driven flow:

$$\langle u^2 \rangle_{\mathrm{m}} = 1.2 g l_0 \langle \rho'^2 / \rho_0^2 \rangle_{t=0}^{\frac{1}{2}}. \tag{6.2}$$

As we have stated $\langle \Theta^2 \rangle$ and $\langle U^2 \rangle$ are computed only from the grid-scale fluctuations, omitting contributions from the subgrid-scale fluctuations. Examination of the energy and buoyancy spectra at large Reynolds numbers (see figures 9–11) indicate that the subgrid contributions to $\langle U^2 \rangle$ may indeed be neglected so that (6.2) is a reliable estimate of the maximum mean-square velocity attained by the fluid. However, owing to a rather slow decrease in the buoyancy spectrum at

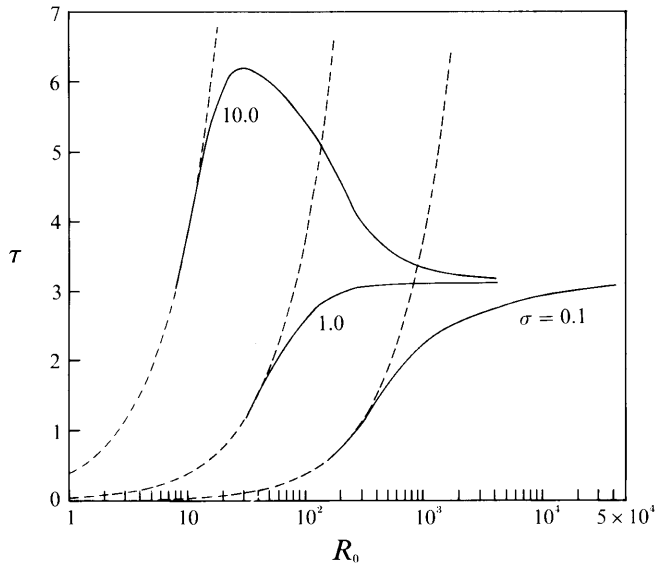

FIGURE 4. The time τ at which $\langle \Theta^2 \rangle$ falls to 0.05 of its initial value as a function of R_0 for $\sigma = 0.1$, 1.0 and 10.0. The dashed lines are the solutions of the linear equations.

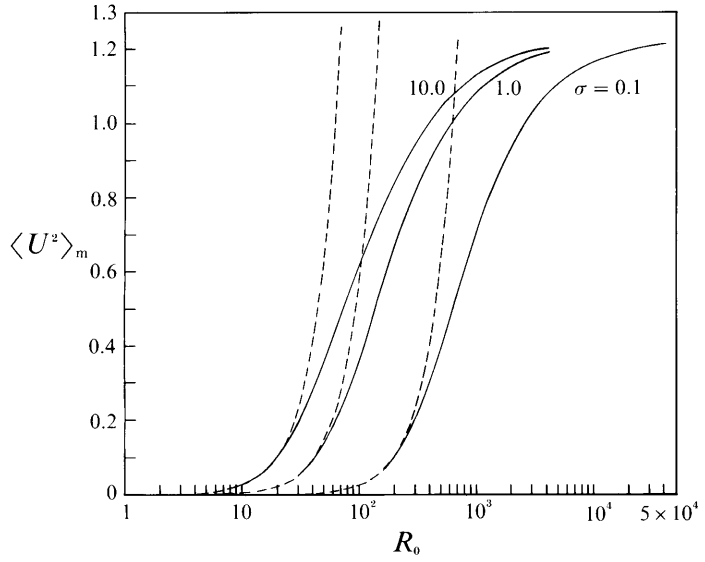

FIGURE 5. The maximum value of $\langle U^2 \rangle$ as a function of R_0 for $\sigma = 0.1$, 1.0 and 10.0. The dashed lines are the solutions of the linear equations.

large wavenumber magnitudes, the subgrid contributions to $\langle \Theta^2 \rangle$ may not be negligible so that the mixing time (6.1) should be considered to be only approximate. We expect the inclusion of subgrid-scale fluctuations to result in somewhat longer mixing times.

Further results for the Prandtl (or Schmidt) number σ equal to 0.1, 1.0, and 10.0 are displayed in figures 4 and 5. The dashed lines are the solutions of the linear equations found in §3. In figure 4, we plot as a function of R_0 the time required for $\langle \Theta^2 \rangle$ to fall to 0.05 of its initial value, while in figure 5 we plot as a function of R_0

the maximum value attained by $\langle U^2 \rangle$. For sufficiently small values of R_0 the linear solutions are recovered, and for sufficiently large values of R_0 the simulation results for all the different values of σ eventually approach the asymptotic results discussed above. In particular, the estimates (6.1) and (6.2) become independent of σ for sufficiently large values of R_0. However, for the asymptotic results to be attained, a larger value of R_0 is required for the smallest value of σ simulated ($\sigma = 0.1$) since both the viscous and diffusive sinks of energy must be negligible over a wide range of inertial wavenumbers. The strength of these sinks depends on the inverses of the Reynolds number R_0 and Péclet number σR_0 respectively, so that both R_0 and σR_0 must be large; and since $\sigma R_0 \ll R_0$ when the Schmidt number is much less than unity, larger values of R_0 are required as σ approaches zero.

The results for the mixing time τ presented in figure 4 for $\sigma = 10.0$ deserve additional comment. The time required for mixing no longer increases monotonically with increasing R_0. There now exists a distinct maximum in the mixing time τ near $R_0 = 32$. It appears that near this value of R_0, turbulent mixing of the large-scale density fluctuations becomes important relative to the weak direct effects of molecular diffusion; and as R_0 increases further, the asymptotic $R \to \infty$ result is approached from above.

It is of interest to determine the effect of varying the width of the spherical shell in which the initial density spectrum is non-zero. Accordingly, we have performed additional simulations with $R_0, \sigma R_0 \to \infty$, and with n varying from 2 to 64 in (5.1). In figure 6, we plot the time evolution of $\langle \Theta^2 \rangle$ and $\langle U^2 \rangle$. As n increases from 2 to 64, the effect on the evolution of $\langle \Theta^2 \rangle$ is small and the maximum value attained by $\langle U^2 \rangle$ increases only by 10%. However, any increase of $\langle U^2 \rangle_m$ with increasing n may be regarded as surprising in the light of our earlier results in §3, where we showed that, for an initial sinusoidal distribution of Θ with wavenumber magnitude κ, $\langle U^2 \rangle$ increases to a maximum value proportional to κ^{-2} before decreasing to zero. For small values of n, many more Fourier components at small κ are excited so that one naïvely expects a corresponding increase in $\langle U^2 \rangle$. In fact, solution of the linearized equations in §3.2 showed that $\langle U^2 \rangle$ diverges as $T \to \infty$ for the particular case $n = 2$. In the simulation such a divergence is seen to be eliminated by nonlinear effects. Furthermore, the unexpected increase in the maximum values of $\langle U^2 \rangle$ with increasing n can be understood upon realizing that the time required for the individual Fourier components of the velocity field to reach their maximum magnitude is proportional to κ^{-2}, so that nonlinear effects already result in a decrease in $\langle U^2 \rangle$ before the growth in the low-wavenumber Fourier components dominates. This is evident from figure 6(*b*), where, for example, $\langle U^2 \rangle$ for $n = 2$ does eventually become larger than $\langle U^2 \rangle$ for $n = 4$.

7. Numerical results for the asymptotic state of the flow field

In this section, we explore the consequences of different initial large-scale density fields on the long-time behaviour of the flow. We have already seen in §§3 and 4 that different power-law forms for $G(\kappa, 0)$ at small κ can lead to very different behaviour of the flow as $T \to \infty$. Furthermore, the results of those sections strongly suggest the existence of an asymptotic similarity state for the particular initial density spectrum given by $n = 2$ in (5.1). One of the consequences of this asymptotic similarity state is that the current Reynolds number of the flow R_t increases indefinitely in time. We are interested in the simulation results for asymptotically large times and this presents difficulties for a direct numerical simulation. Accordingly, we have

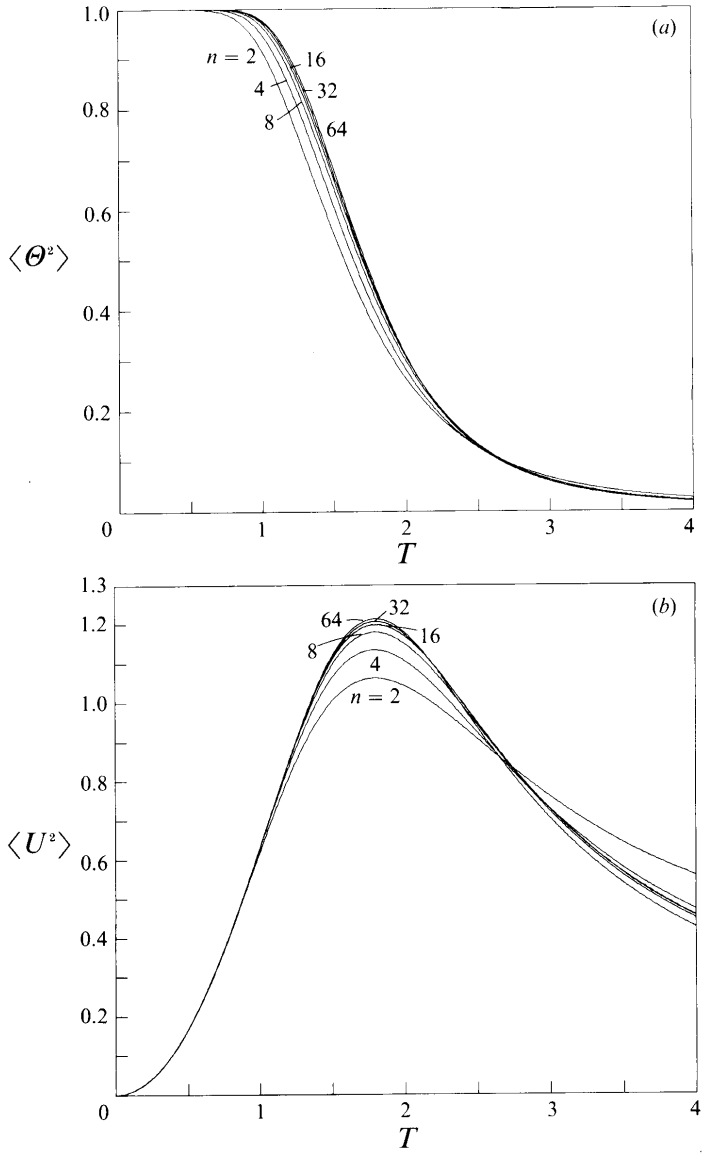

FIGURE 6. Effect of varying the width of the initial density spectrum by varying n in (5.1), for R_0, $\sigma R_0 \to \infty$: (*a*) $\langle \Theta^2 \rangle$ *vs.* T, (*b*) $\langle U^2 \rangle$ *vs.* T.

performed large-eddy simulations with $R_0, \sigma R_0 \to \infty$ with resolution 128^3 and the maximum of the density spectrum occurring at a computational wavenumber magnitude of $k_p = 50$. However, as discussed in §6, the choice of such a large value for k_p in the simulation can lead to erroneous results. In particular, an overdamping of the fields by the subgrid model occurs over the times at which the turbulent velocity of the fluid increases. This overdamping leads to an underestimation of the maximum mean-square velocity of the fluid. However, this need not concern us unduly here since accurate statistical results for the maximum mean-square velocities have already been obtained in §6 and, more importantly, the similarity properties at large times should not be altered by an overdamping of the fields at early times.

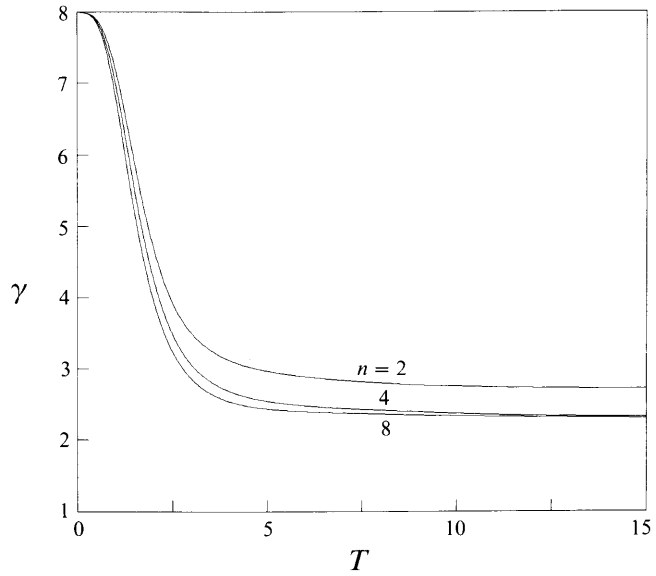

FIGURE 7. Time evolution of the anisotropy factor γ for $G(\kappa, 0)$ given by (5.1) with $n = 2$, 4 and 8.

As a measure of the large-scale anisotropy of the velocity field at large values of T, we plot in figure 7 the time evolution of the parameter

$$\gamma = \frac{2\langle U_3^2 \rangle}{\langle U_1^2 \rangle + \langle U_2^2 \rangle}. \tag{7.1}$$

The linearized equations predict a value for γ equal to eight (see (3.8)), whereas isotropic turbulence would have γ equal to unity. Asymptotically as $T \to \infty$, we find that γ is approximately 2.8 for $n = 2$, whereas γ is approximately 2.4 for $n = 4$ and 8. Thus, the velocity field in the final period of decay is more isotropic than that determined by the linearized equations, yet still remains far from isotropy even though the flow becomes quite turbulent. The difference in the asymptotic values of γ for different n is evidently a consequence of the differing degrees of isotropy of the large-scale density fields. For $n = 2$, the leading term in the expansion of $\Psi(\boldsymbol{\kappa}, T)$ in powers of $\boldsymbol{\kappa}$ is necessarily isotropic for all T, whereas for $n = 4$ and 8, the leading term is determined by anisotropic nonlinear interactions. Note that the approach of γ to a constant at large times for each value of n provides the first direct evidence of the existence of an asymptotic similarity state at large times.

In figure 8, the time evolution of $\langle \Theta^2 \rangle$, $\langle U^2 \rangle$, and L_t in the three cases $n = 2$, 4, and 8 is presented. The non-dimensional current lengthscale L_t is taken to be representative of the scales making up the maximum contribution to $\langle \Theta^2 \rangle$ at time T and is defined as

$$L_t = 2\pi B_n \langle \Theta^2 \rangle^{-1} \int_0^\infty \kappa^{-1} G(\kappa, T)\, \mathrm{d}\kappa. \tag{7.2}$$

Here B_n is chosen so that $L_t = 1$ at $T = 0$, whence

$$B_n = \frac{2(\frac{1}{2}n)^{\frac{1}{2}n}}{A_n(\frac{1}{2}n-1)!} \tag{7.3}$$

and A_n is given by (5.2). The main results of interest are the power-law functional

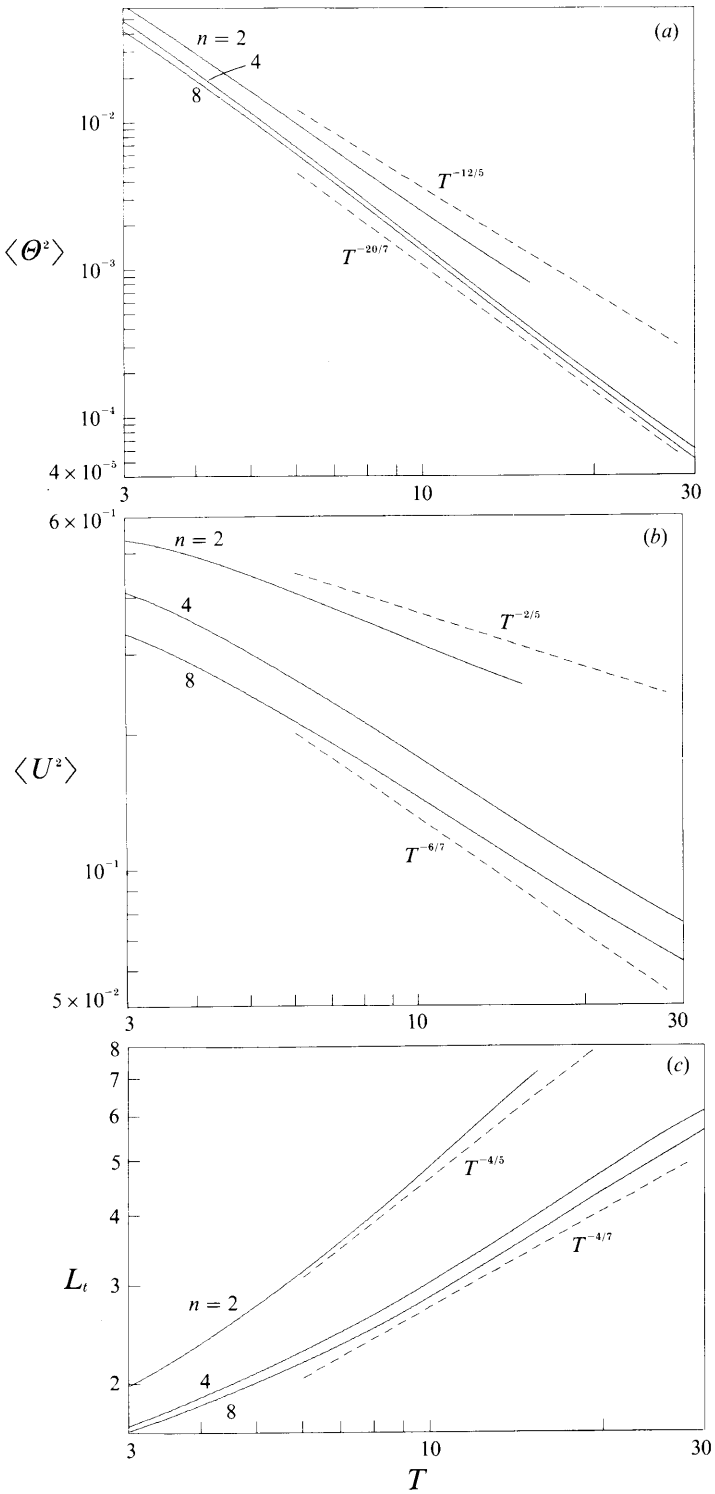

FIGURE 8. Numerical results for the asymptotic similarity state when $R_0, \sigma R_0 \to \infty$ and $G(\kappa, 0)$ is given by (5.1) with $n = 2$, 4, and 8: (*a*) $\langle \Theta^2 \rangle$ *vs.* T, (*b*) $\langle U^2 \rangle$ *vs.* T, (*c*) L_t *vs.* T. The slopes found theoretically for $n = 2$ and empirically for $n = 4$, 8 are shown for comparison as broken lines.

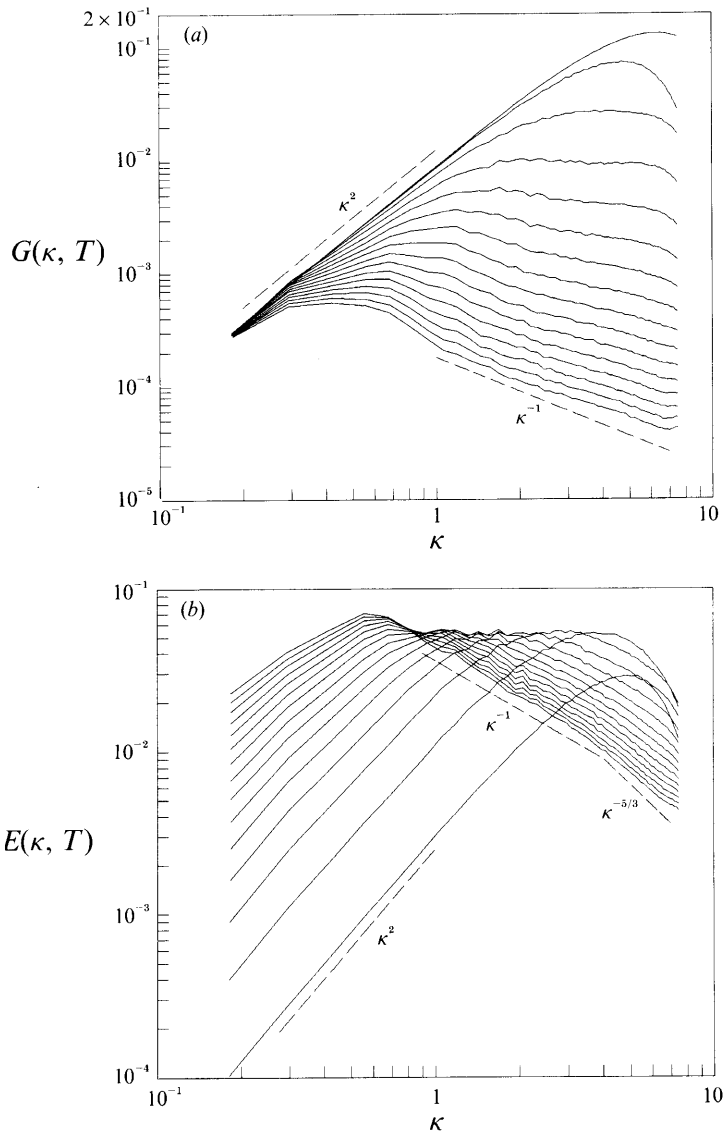

FIGURE 9. Evolution from $T = 0$ to 15 of the density and energy spectra when $R_0, \sigma R_0 \to \infty$ and $G(\kappa, 0)$ is given by (5.1) with $n = 2$: (*a*) $G(\kappa, T)$ *vs.* κ, (*b*) $E(\kappa, T)$ *vs.* κ.

forms in the asymptotic similarity state. The theoretical results obtained in §4 for $n = 2$ are plotted in figure 8 alongside the simulation results, and the slopes are seen to be in reasonable agreement. We have also plotted suggested asymptotic power laws alongside the simulation results for $n = 4$ and 8. Further discussion of these empirical asymptotic power laws will be found below.

The time evolution of the density spectrum $G(\kappa, T)$ and the energy spectrum $E(\kappa, T)$, defined in (4.10), for $n = 2$ is shown in figure 9. As is immediately evident from the graph of $G(\kappa, T)$ (figure 9*a*), the theoretical prediction that C_0 in (4.5) is constant is well obeyed by the numerical simulation spectrum. As explained in §4, the invariance of C_0 gives rise to the asymptotic similarity relations for $n = 2$ shown in figure 8.

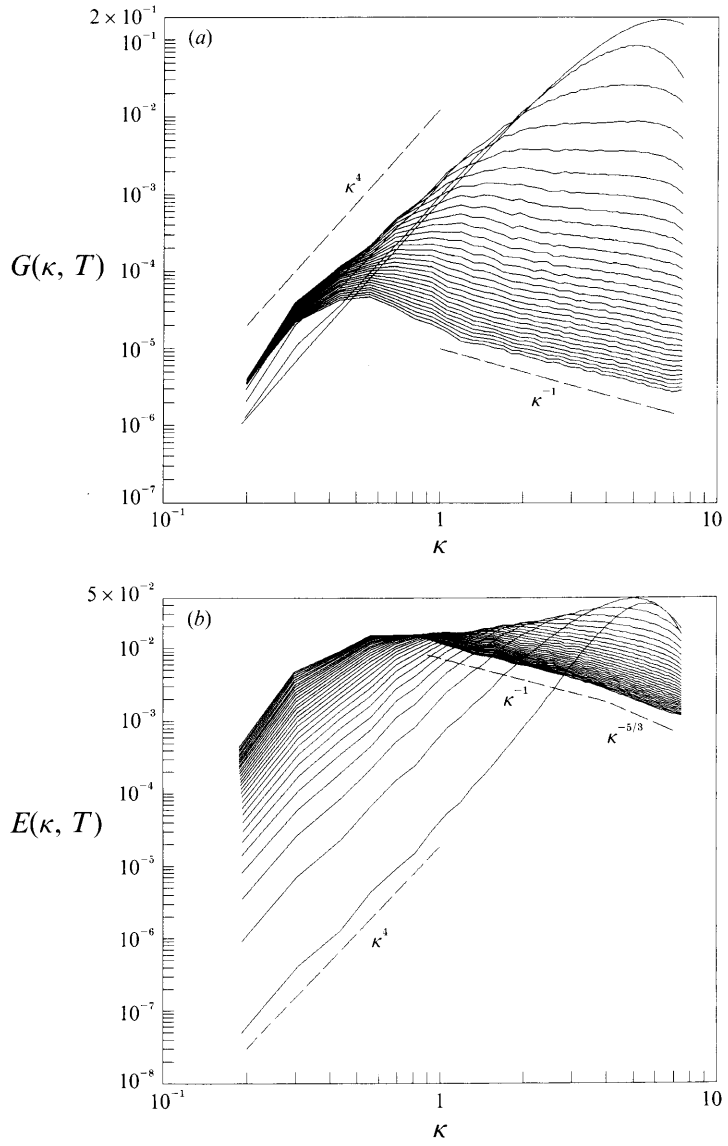

FIGURE 10. Evolution from $T = 0$ to 30 of the density and energy spectra when R_0, $\sigma R_0 \to \infty$ and $G(\kappa, 0)$ is given by (5.1) with $n = 4$: (*a*) $G(\kappa, T)$ *vs.* κ, (*b*) $E(\kappa, T)$ *vs.* κ.

The time evolution of the spectra for $n = 4$ and 8 is shown in figure 10 and 11, respectively. We observe the development of a κ^4 form for $G(\kappa, T)$ at small κ as predicted in §4. The coefficient in this κ^4-spectrum, namely

$$C_2 = \lim_{\kappa \to 0} G(\kappa, T)/4\pi\kappa^4, \tag{7.4}$$

is not invariant according to the theory in §4, unlike the coefficient C_0, and changes in its value at early times are evident in figures 10(*a*) and 11(*a*). For later times, however, C_2 is observed to vary much more slowly with time.

The near invariance of the coefficient C_2 at later times raises the question whether there exists an 'empirical' asymptotic similarity state when $n \geqslant 4$. If we assume C_2

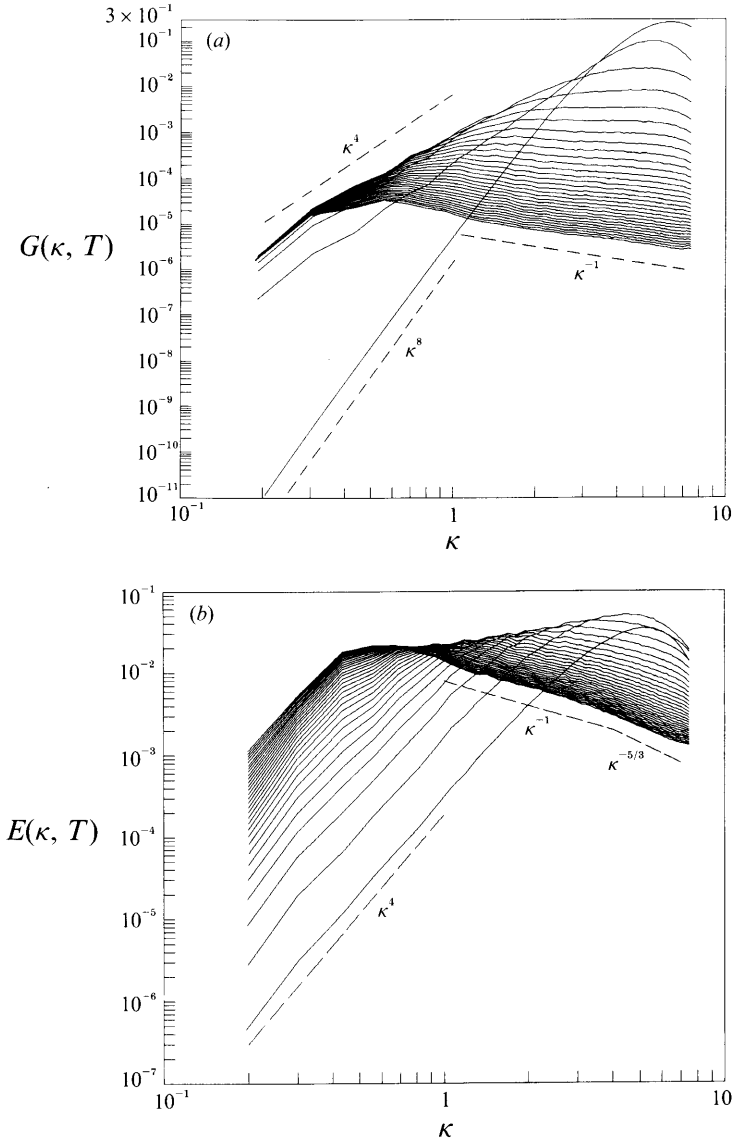

FIGURE 11. As for figure 10 but with $n = 8$.

to be invariant in this asymptotic similarity state, and further assume it to be the only parameter needed to determine the flow, we find analogously to the scaling of (4.14)

$$\langle \Theta^2 \rangle \propto T^{-\frac{20}{7}}, \quad \langle U^2 \rangle \propto T^{-\frac{6}{7}}, \quad L_t \propto T^{\frac{4}{7}}. \tag{7.5}$$

These asymptotic relations have been plotted alongside the results of the simulations for $n = 4$ and 8 in figure 8 and the slopes are seen to be in reasonable agreement.

The asymptotic relations (7.5) can be used to obtain asymptotic similarity forms for the density and energy spectra which are analogous to those in (4.15). Defining these similarity functions by $\hat{G}(\hat{\kappa})$ and $\hat{E}(\hat{\kappa})$, we obtain for $n \geqslant 4$

$$G(\kappa, T) = T^{-\frac{16}{7}} \hat{G}(\hat{\kappa}), \quad E(\kappa, T) = T^{-\frac{9}{7}} \hat{E}(\hat{\kappa}), \quad \hat{\kappa} = T^{\frac{4}{7}} \kappa. \tag{7.6}$$

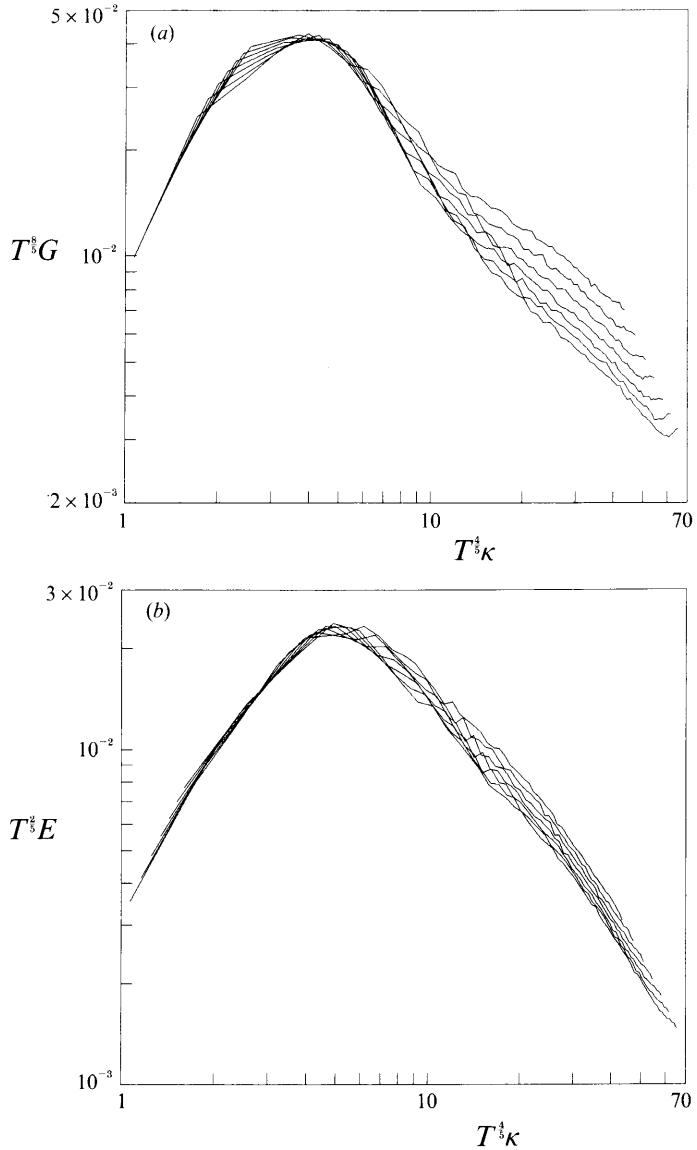

FIGURE 12. As for figure 9 (in which $n = 2$) but with $T = 9$ to 15 and the spectra rescaled according to the theoretical asymptotic similarity relations (4.15).

The spectra for $n = 2$ and 4 have been rescaled at the later times of the simulations according to (4.15) and (7.6) and are plotted in figures 12 and 13, respectively. A reasonable collapse of the spectra is observed for wavenumber magnitudes lying in the range containing most of the energy and density-variance.

It seems therefore that the approximate invariance of C_2 at large times when $C_0 = 0$ is accompanied by a similarity state, and that this state is different from that for $n = 2$. We have not been able to find a physical interpretation of the approximate invariance of C_2.

Finally, we note the approximate power-law forms of the spectra at large wavenumber magnitudes in figures 9–11. In all the simulations, the density spectra $G(\kappa, T)$ are slightly less steep than κ^{-1} at large κ. A κ^{-1}-spectrum at large κ for a

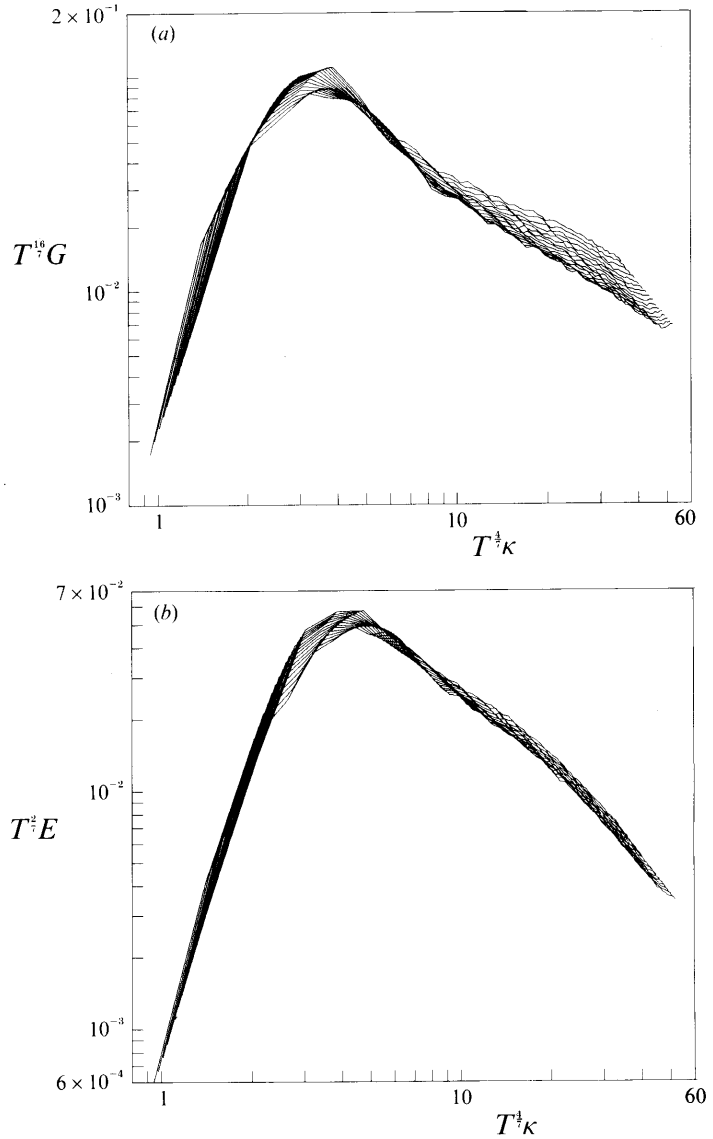

FIGURE 13. As for figure 10 (in which $n = 4$) but with $T = 15$ to 30 and the spectra rescaled according to the empirical asymptotic similarity relations (7.6).

passive scalar field in isotropic turbulence was previously found numerically by Lesieur & Rogallo (1989), although it is unclear if our buoyancy-generated turbulence results are related. The power-law behaviour of the energy spectra is less distinct, but appears to be slightly greater than κ^{-1} immediately after the energy peak, and bends closer to $\kappa^{-\frac{5}{3}}$ for scales near the cutoff wavenumber. However, the limited range of scale sizes available to our 128^3 numerical simulations makes speculative any conclusions concerning these small-scale spectra. Additional analytical and numerical study is required, and we leave this for future work.

8. A model for the turbulent transport processes

We have found herein an analytical representation of both the initial growth and the final decay of velocity fluctuations in homogeneous buoyancy-generated turbulence by means of a linear analysis of the fundamental equations and the discovery of asymptotic similarity states, respectively. Results of the numerical simulations have confirmed the validity of these analytical representations at small and large times. However, we still have no analytical representation for the results of the numerical simulations at intermediate times, in particular at times near that at which the mean-square velocity fluctuation attains a maximum value when R_0 is large. We show here that a rough analytical representation of this feature of the flow can be obtained by modelling the turbulent transport of kinetic energy and density-variance from large to small scales.

From the governing equations in dimensional form, (2.4), (2.5) and (2.6), we find

$$\frac{1}{2}\frac{\mathrm{d}\langle u^2\rangle}{\mathrm{d}t} = \frac{g}{\rho_0}\langle u_3\rho'\rangle + \nu\langle \boldsymbol{u}\cdot\nabla^2\boldsymbol{u}\rangle, \tag{8.1}$$

$$\frac{1}{2}\frac{\mathrm{d}\langle \rho'^2\rangle}{\mathrm{d}t} = D\langle \rho'\nabla^2\rho'\rangle \tag{8.2}$$

when $\boldsymbol{u}$ and ρ' are statistically homogeneous. Now at large Reynolds numbers the length scales at which molecular dissipation occurs are much smaller than the scale l_t of the energy-containing eddies, and these small-scale components of $\boldsymbol{u}$ and ρ' exist solely as a consequence of nonlinear transfer of kinetic energy and density-variance from the large scales near l_t. A widely tested expression for the rate at which kinetic energy is transferred to smaller scales is $\alpha\langle u^2\rangle^{\frac{3}{2}}/l_t$, where $\frac{1}{2}\langle u^2\rangle$ is the kinetic energy per unit mass associated with scales near l_t and α is a positive constant not far from unity (Batchelor 1953, §6.1). Provided this transfer of energy is rapid, $\alpha\langle u^2\rangle^{\frac{3}{2}}/l_t$ must also be the instantaneous rate at which energy is being lost from the small scales by viscous dissipation, whence (8.1) can be written as

$$\frac{1}{2}\frac{\mathrm{d}\langle u^2\rangle}{\mathrm{d}t} = \frac{g}{\rho_0}\langle u_3\rho'\rangle - \frac{\alpha\langle u^2\rangle^{\frac{3}{2}}}{l_t}. \tag{8.3}$$

The analogous expression for the rate at which density-variance is being transferred by nonlinear convection processes from scales near l_t to small scales is $\beta\langle u^2\rangle^{\frac{1}{2}}\langle \rho'^2\rangle/l_t$, whence by similar arguments we may rewrite (8.2) as

$$\frac{1}{2}\frac{\mathrm{d}\langle \rho'^2\rangle}{\mathrm{d}t} = -\frac{\beta\langle u^2\rangle^{\frac{1}{2}}\langle \rho'^2\rangle}{l_t}, \tag{8.4}$$

where β is another constant of order unity.

We also introduce ζ, the coefficient of correlation between ρ' and the vertical component of velocity, u_3, defined by

$$\langle \rho' u_3\rangle = \zeta\langle \rho'^2\rangle^{\frac{1}{2}}\langle u_3^2\rangle^{\frac{1}{2}}, \tag{8.5}$$

and the factor γ, a measure of the anisotropy of the energy-containing eddies, defined in (7.1). For a flow field resulting from an initially isotropic density distribution, the initial values of ζ and γ are $(5/6)^{\frac{1}{2}}$ and 8, respectively. At later times, after the flow

has become turbulent, the values of ζ and γ may both be expected to be smaller because the fluid velocity is less closely controlled by gravity when inertia forces are strong.

Equation (8.3) thus becomes

$$\frac{\mathrm{d}\langle u^2\rangle^{\frac{1}{2}}}{\mathrm{d}t} = \frac{g\xi}{\rho_0}\langle \rho'^2\rangle^{\frac{1}{2}} - \frac{\alpha\langle u^2\rangle}{l_t}, \tag{8.6}$$

where $\xi = \zeta\gamma^{\frac{1}{2}}/(2+\gamma)^{\frac{1}{2}}$. If now we make the convenient approximations that the factor ξ and the lengthscale l_t of the eddies making the main contributions to $\langle u^2\rangle$ and $\langle \rho'^2\rangle$ are both constant, we may eliminate $\langle \rho'^2\rangle^{\frac{1}{2}}$ from (8.4) and (8.6) to obtain

$$\frac{\mathrm{d}^2\langle u^2\rangle^{\frac{1}{2}}}{\mathrm{d}t^2} + \frac{\alpha+\frac{1}{2}\beta}{l_t}\frac{\mathrm{d}\langle u^2\rangle}{\mathrm{d}t} + \frac{\alpha\beta}{l_t^2}\langle u^2\rangle^{\frac{3}{2}} = 0, \tag{8.7}$$

with initial conditions

$$\langle u^2\rangle^{\frac{1}{2}}_{t=0} = 0, \quad \left.\frac{\mathrm{d}\langle u^2\rangle^{\frac{1}{2}}}{\mathrm{d}t}\right|_{t=0} = \xi g\frac{\langle \rho'^2\rangle^{\frac{1}{2}}_{t=0}}{\rho_0} = \xi g\theta_0, \tag{8.8}$$

the second condition being determined directly from (8.6).

Remarkably, (8.7) and (8.8) admit the analytical solution

$$\langle u^2\rangle^{\frac{1}{2}} = \frac{\xi g\theta_0 t}{1+\frac{1}{2}\alpha^{\frac{1}{2}}\beta^{\frac{1}{2}}\xi(g\theta_0 t^2/l_t)}, \tag{8.9}$$

provided that α/β, which may be seen from (8.3) and (8.4) to be a kind of turbulent Schmidt number, has either of the values 1 or $\frac{1}{4}$. The corresponding expression for $\langle \rho'^2\rangle$ is

$$\frac{\langle \rho'^2\rangle^{\frac{1}{2}}}{\rho_0} = \frac{\theta_0}{\{1+\frac{1}{2}\alpha^{\frac{1}{2}}\beta^{\frac{1}{2}}\xi(g\theta_0 t^2/l_t)\}^{\beta^{\frac{1}{2}}/\alpha^{\frac{1}{2}}}}. \tag{8.10}$$

In terms of the dimensionless variables defined in §2, (8.9) and (8.10) become

$$\langle U^2\rangle^{\frac{1}{2}} = \frac{\xi T}{1+\frac{1}{2}\alpha^{\frac{1}{2}}\beta^{\frac{1}{2}}\xi T^2}, \quad \langle \Theta^2\rangle^{\frac{1}{2}} = \frac{1}{(1+\frac{1}{2}\alpha^{\frac{1}{2}}\beta^{\frac{1}{2}}\xi T^2)^{\beta^{\frac{1}{2}}/\alpha^{\frac{1}{2}}}}. \tag{8.11}$$

From (8.11), we find the maximum mean-square velocity attained by the fluid and the time at which it occurs to be

$$\langle U^2\rangle_{\mathrm{m}} = \frac{\xi}{2\alpha^{\frac{1}{2}}\beta^{\frac{1}{2}}}, \quad T_{\mathrm{m}} = \frac{\sqrt{2}}{\xi^{\frac{1}{2}}\alpha^{\frac{1}{4}}\beta^{\frac{1}{4}}}. \tag{8.12}$$

Assuming $\xi = (2/3)^{\frac{1}{2}}$ as for a viscous-dominated flow field, and $\alpha = \beta$, the model is compatible with the numerical simulation result $T_{\mathrm{m}} = 1.8$ found in §6 if $\alpha = \beta = 0.76$. The corresponding model value for $\langle U^2\rangle_{\mathrm{m}}$ is 0.54, about a factor of two less than the numerical simulation result 1.2, and the dimensionless mixing time τ defined in §6 is 3.3 whereas the simulation gives 3.1.

The two model relations in (8.11) with the reasonable parameter values $\alpha = \beta = 0.76$ and $\xi = (2/3)^{\frac{1}{2}}$ are plotted in figure 14, and are compared there with the

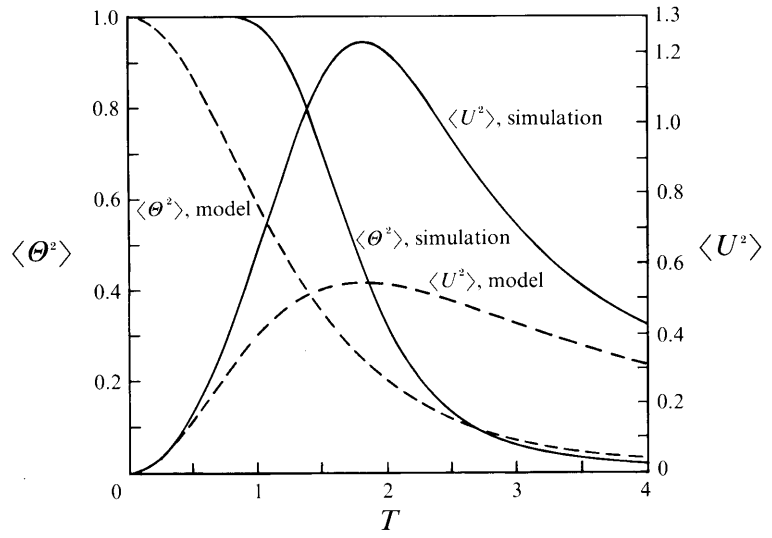

FIGURE 14. Comparison of the results of the numerical simulation for $R_0, \sigma R_0 \to \infty$ and $G(\kappa, 0) = \delta(\kappa - 2\pi)$ (see §6) with those given by the model equation (8.7).

results of the numerical simulation for large R_0 described in §6. The correspondence is acceptable qualitatively, and suggests that our representation of the turbulent transport processes in the model may be adequate for some approximate purposes.

The authors would like especially to thank Dr R. Rogallo for supplying his numerical simulation code as well as for his many helpful comments and suggestions over the course of this research. We would also like to thank J. Jonas for making available his flow visualization software, P. Pazos for her help in preparing the colour plate, and J. Mendoza for his drafting of the figures.

All the simulations presented in this paper were performed using the computational facilities of the NASA Ames Research Center. Part of this research was done during the 1990 NASA Ames/Stanford Center for Turbulence Research Summer Program. One of the authors (J. R. C.) gratefully acknowledges partial support from the NASA Ames Research Center and from the National Research Council – NASA Goddard Institute for Space Studies Research Associateship program.

REFERENCES

BATCHELOR, G. K. 1963 *The Theory of Homogeneous Turbulence*. Cambridge University Press.

BATCHELOR, G. K. & PROUDMAN, I. 1956 The large-scale structure of homogeneous turbulence. *Phil. Trans. R. Soc. Lond.* **248**, 369–405.

CHASNOV, J. R. 1991 Simulation of the Kolmogorov inertial subrange using an improved subgrid model. *Phys. Fluids* A **3**, 188–200.

CHOLLET, J. P. 1985 Two-point closure used for a sub-grid scale model in large eddy simulations. In *Turbulent Shear Flows IV* (ed. L. J. S. Bradbury *et al.*), pp. 62–72.

CHOLLET, J. P. & LESIEUR, M. 1981 Parameterization of small scales of three-dimensional isotropic turbulence utilizing spectral closures. *J. Atmos. Sci.* **38**, 2747–2757.

GIBSON, C. H. 1986 Internal waves, fossil turbulence, and composite ocean microstructure spectra. *J. Fluid Mech.* **168**, 89–117.

KRAICHNAN, R. H. 1976 Eddy viscosity in two and three dimensions. *J. Atmos. Sci.* **33**, 1521–1536.

LESIEUR, M. & ROGALLO, R. 1989 Large-eddy simulation of passive scalar diffusion in isotropic turbulence. *Phys. Fluids* A **1**, 718–722.

MÉTAS, O. & CHOLLET, J. P. 1989 Turbulence submitted to a stable density stratification: large-eddy simulations and statistical theory. In *Turbulent Shear Flows VI* (ed. J.-C. André *et al.*), pp. 398–416. Springer.

ROGALLO, R. S. 1981 Numerical experiments in homogeneous turbulence. *NASA TM* 81315.

SAFFMAN, P. G. 1967 The large-scale structure of homogeneous turbulence. *J. Fluid Mech.* **27**, 581–593.